Behavior of Cs^+-UF_6^- ion-pair plasmas in radiofrequency quadrupole-dipole fields. I. Experiment[a)]

S. Wexler, E. K. Parks, C. E. Young, and R. A. Bennett[b)]
Chemistry Division, Argonne National Laboratory, Argonne, Illinois 60439

(Received 5 August 1982; accepted for publication 28 October 1982)

The behavior of a flowing Cs^+-UF_6^- ion-pair plasma in the radiofrequency (rf) quadrupole-dipole fields of a mass filter has been studied experimentally. The flowing plasma was formed by collision of a beam of accelerated UF_6 molecules with an intense beam of thermal Cs atoms. The maximum current (positive- or negative-ion flux) entering the mass filter was 0.5×10^{-3} A, corresponding to a positive- or negative-ion density in the injection region of $\sim1.1\times10^{10}$ ions/cm^3. Four aspects of the interaction of the plasma with the radiofrequency fields were investigated: (1) the injection of the ion-pair plasma into the quadrupole-dipole field, (2) confinement by and transmission of the flowing plasma through a quadrupole field, (3) mass-sensitive ejection of ions from the plasma by superimposed quadrupole and dipole fields, and (4) effects of the extraction and exit fringe fields on the flowing plasma. In particular, the effects of increasing plasma density in relation to the above topics was experimentally determined. The results of the experimental observations in conjunction with the theoretical calculations discussed in the following paper suggest that the limiting-ion flux that can be confined within a quadrupole mass filter is determined by the requirement that the plasma frequency ν_p must be lower than or at most equal to the applied rf quadrupole frequency ν_1. If $\nu_p > \nu_1$, the rf field causes rapid destruction of the plasma. The mass-resolving power of the mass filter was found to deteriorate significantly with increasing plasma throughput, a result of the increasing space-charge forces within the plasma and their interaction with the applied dipole field.

PACS numbers: 52.55.Mg, 41.80.Gg, 82.20.Fd

I. INTRODUCTION

Practical methods of isotope separation based on the mass separation of ions require some method of overcoming the space-charge limitation on the intensity of ion beams. One obvious technique, used, for example, on the calutron isotope separator,[1] is to operate with ion beams at high kinetic energies such that space-charge blowup of the beams is kept within reasonable bounds. In this paper, we consider another method, based on neutralizing the space charge within the ion beam of interest with a confluent beam of oppositely charged ions, thus forming a flowing ion-pair plasma.

In the present study, a flowing $Cs^+ - UF_6^-$ plasma was formed by colliding an intense beam of accelerated UF_6 molecules with an intense beam of thermal Cs atoms, whereby ion pairs are formed by the efficient electron-transfer process. Mass separation of the $^{235}UF_6^-$ ions from the $^{238}UF_6^-$ was accomplished by passing the flowing ion-pair plasma through a radiofrequency (rf) quadrupole mass filter (QMF) operated in the ion-ejection mode. In this mode of operation, an rf quadrupole field is applied to the mass filter (with *no* dc component) to confine all ions which fall within the appropriate stability diagram. A weak rf dipole field is then superimposed on the quadrupole field to eject a specific ion mass, in the present case $^{238}UF_6^-$ (for a more complete discussion of the ion-ejection mode, see the following paper,[2] Paper II, Secs. II and V). The use of a flowing quasineutral plasma in place of a beam of uniformly charged species was expected to permit the transmission of ion fluxes greatly exceeding the limits imposed by space-charge forces.

In the course of the development effort on this approach, we examined four aspects of the interactions of the Cs^+-UF_6^- plasma with rf fields, which are the subject of this paper: (1) the injection of the ion-pair plasma into a quadrupole-dipole field, (2) confinement and transmission of the flowing plasma through a quadrupole field, (3) mass-sensitive ejection of ions from the plasma by superimposed quadrupole and dipole fields, and (4) effects of the extraction and exit fringe fields on the flowing plasma. Each of the above is strongly dependent on the density of the injected plasma, and it is this dependence that is of particular interest.

Two primary questions were at the core of this research effect. First, what are the throughput limitations associated with transporting a plasma through a QMF? This is primarily related to the relative importance of the applied rf quadrupole field, which tends to confine the ions within the mass filter, and the space-charge forces within the plasma itself, which tend to disrupt the confining action of the applied field. Second, how does the presence of space-charge forces within the plasma affect the mass-resolving power of the mass filter? Evidence on the mass resolution comes directly from the experimental results, although theory and experiment are in general agreement on the observed effects. An upper limit on plasma throughput, however, is only sug-

[a)] This work was supported principally by the Advanced Nuclear Systems and Projects Division, Advanced Isotope Separations Branch, and also by the Office of Basic Energy Sciences, Division of Chemical Sciences, U.S. Department of Energy, under Contract W-31-109-Eng-38.

[b)] Present address: CAI/Bourns Company, Barrington, Il. 60010.

 0021-8979/83/041730-25$02.40

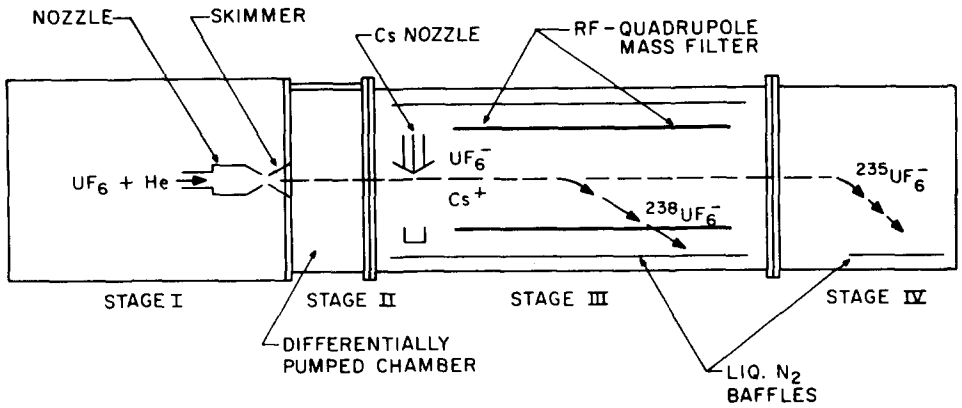

FIG. 1. Schematic of the apparatus.

gested by the experimental results, and in this case the theoretical calculations (discussed in Paper II) demonstrate more clearly the presence of and the reasons for a throughput limitation.

Ion-pair plasmas have received little attention in the past, most likely because of the difficulties in producing sufficient densities of ion pairs to constitute a plasma. Formation of low-density plasmas by relatively inefficient photodissociation of diatomic molecule to ion pairs has been reported.[3–5] Moderately dense plasmas containing I^+ and I^- have been prepared by introducing molecular iodine into electrical discharges,[6,7] and the characteristics of a low-density Tl^+-I^- ion-pair plasma confined in a quadrupole-ion trap have been examined by Schermann and Major.[8] The meager literature on ion-pair plasmas is, of course, in sharp contrast to that on electron-positive ion plasmas, which have been extensively studied for many years.

In Sec. II of this paper, we present a brief outline of the experimental apparatus and the types of measurements made. In Sec. III, the apparatus is considered in detail, and in Sec. IV, the formation of the ion-pair plasma and its injection into the mass filter is discussed. Sections V and VI contain the experimental results not specificially related to isotope separation, while Sec. VII gives the results of experiments designed to separate $^{238}UF_6^-$ from $^{235}UF_6^-$. A discussion of all the experimental results and their relation to the theoretical calculations is given in Sec. VIII. For a more detailed discussion of the theoretical results, the reader is referred to Paper II.[2]

II. BRIEF DESCRIPTION OF THE EXPERIMENT

In this section, a brief description of the experiment is presented, which will serve to orient the reader for the more detailed description which follows.

The experimental apparatus consists of four stages, schematically depicted in Fig. 1. Stages I and II are designed to produce a high-intensity beam of UF_6 molecules of sufficient energy to exceed the threshold for the reaction $Cs + UF_6 \rightarrow Cs^+ + UF_6^-$ for a thermal Cs target (the laboratory threshold is <0.3 eV).[9] Acceleration of UF_6 is by the seeded jet method,[10] in which the UF_6 is added in low concentration to a light carrier gas (either H_2 or He), and the mixture is expanded out of a nozzle at elevated temperature and pressure. Stage I is pumped by a large blower/mechanical pump combination to remove the rather large quantities of carrier gas which exit from the nozzle. Specially designed liquid-N_2 traps remove the UF_6 from the carrier gas before the gas flow reaches the pumping system.

The core of the nozzle output is skimmed off by a conical skimmer, and passes into Stage II. Stage II serves to isolate the high pressure of Stage I from the low pressure required in Stage III. After being further collimated on the downstream wall of Stage II, the collimated UF_6 beam passes into Stage III.

In Stage III, the UF_6 beam intercepts a crossed beam of thermal Cs atoms, and the resulting electron-transfer reaction produces a flowing ion-pair plasma, which then *drifts* through a quadrupole mass filter. (Actually the drift is along the center-of-mass motion of the two ions, but owing to the large kinetic energy of the UF_6 molecules compared to that of the Cs atoms, the center-of-mass motion is closely aligned with the UF_6 beam axis.) The problems associated with passing a relatively slow-moving plasma through the entrance and exit fringe fields of the QMF are of considerable importance, and constitute a significant part of our experimental observations. Two experimental arrangements have been tested, one in which the ion-pair plasma is formed just upstream from the entrance of the QMF, and the other in which the ion-pair plasma is formed just inside the entrance to the QMF itself (see Sec. IV).

The rf QMF is approximately 100 cm long and has a 5-cm field radius. Its poles are constructed of strung wires, both for ease of construction and to maintain adequate pumping through the sides of the unit. It is surrounded by liquid-N_2 baffles to insure a low pressure of background UF_6 within the QMF itself. Voltages in excess of 20 kV can be applied to the four poles of the mass filter. Either the Cs^+ or UF_6^- which is transmitted through the device can be measured by means of collection plates and an associated lens system for focusing, which are located downstream from the exit of the mass filter.

Stage IV is used for various diagnostic measurements on the UF_6 primary beam, as well as for measurements of the isotopic distribution of the UF_6^- transmitted through the mass filter.

Two types of experimental measurements were made: (1) studies of plasma confinement within the QMF operating with only an rf quadrupole field, and (2) studies of mass-sensitive ejection of ions by the simultaneous application of

both a quadrupole and a dipole field. Confinement of the plasma has been studied under conditions where both the Cs^+ and UF_6^- are in stable orbits (in the low-density limit), as well as under conditions where the UF_6^- is stable but the Cs^+ is not. A typical experiment involved determining the throughput (i.e., the Cs^+ or UF_6^- flux exiting the mass filter) as a function of the magnitudes of the applied rf quadrupole and dipole field strengths for fixed quadrupole and dipole frequencies and a fixed flux of the injected plasma.

III. EXPERIMENTAL APPARATUS

A. Stage I

The function of Stages I and II is to provide an intense beam of accelerated UF_6 molecules. The acceleration is obtained by means of the seeded-jet technique, whereby UF_6 molecules are entrained at low concentration in a high-pressure carrier gas (either He or H_2), and the mixture is expanded out of a supersonic nozzle at elevated temperature. Velocity equilibrium of the heavy and light species, which results from the high pressure, insures a kinetic energy enhancement of the heavy species, given by

$$E_{\text{heavy}} = \tfrac{1}{2}M_{\text{heavy}}v^2 = \frac{M_{\text{heavy}}}{M_{\text{light}}}\tfrac{1}{2}M_{\text{light}}v^2 = \frac{M_{\text{heavy}}}{M_{\text{light}}}E_{\text{light}},$$

where M_{heavy} is the mass of UF_6 and M_{light} is the mass of He or H_2. For UF_6 in H_2, the UF_6 kinetic energy is $352/2 = 176$ times that of the H_2. Thus the thermal energy of hydrogen at room temperature will already result in UF_6 molecules with electron volts of kinetic energy.

The Stage I→IV chambers are shown in a scaled drawing (top view) in Fig. 2. The Stage I chamber, which houses the supersonic nozzle and skimmer, is constructed entirely of 6061 aluminum, which has excellent resistance to UF_6 attack. The UF_6-carrier gas mixture, electrical power, and diagnostic devices enter the chamber through flanges on the bottom of the unit. The seeded-jet method generally requires a substantial flow of carrier gas, and consequently a considerable pumping speed for the chamber housing the nozzle. The Stage I pumping system includes a 4000 CFM Kinney Blower (Model KMBD-4000) backed by a 850 CFM Kinney mechanical pump (Model KT850). In addition, Stage I can also be pumped by a 16-in. oil-diffusion pump backed by the above 850 CFM mechanical pump. The diffusion pump and associated liquid-N_2 baffle can be isolated from Stage I by a 16-in. valve when operated with the blower/mechanical pump combination. Owing to the high pumping speed of the latter and the large mass difference between the seed species UF_6 and the carrier gas (H_2 or He), it was possible to form an intense beam of accelerated UF_6 without use of the diffusion pump. At a pressure of 2 atm in the nozzle (0.025-cm-diam aperture), the background pressure in Stage I was typically 0.035 Torr (of which less than 1% was UF_6), and the resultant attenuation of the UF_6 beam was relatively small. Further increase of the UF_6 flux was limited by UF_6 cluster formation and not by pumping speed.

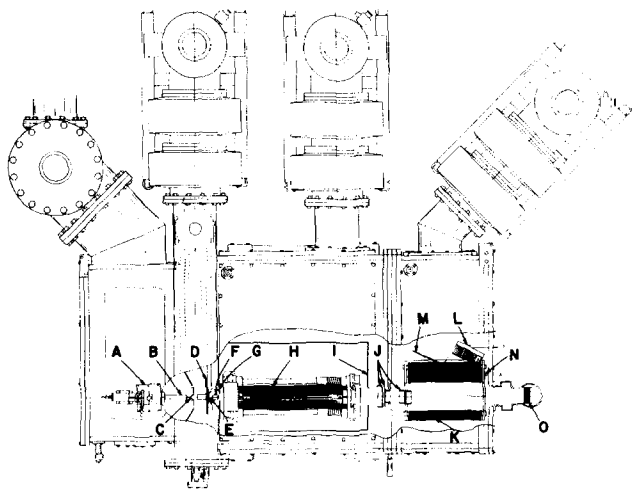

FIG. 2. Scaled drawing of the apparatus—top view. A-three-dimensional control for the nozzle; B-nozzle; C-skimmer; D-chopper; E-collimating aperture; F-Cs source; G-grounded plate; H-quadrupole mass filter; I-liquid-N_2-cooled baffle; J-ion extraction lenses; K-ion deflector; L-sample collector; M-shield for sample collector; N-ion flux monitor; O-liquid-N_2-cooled trap.

A high throughput liquid-N_2 trap was designed to separate the UF_6 from the He or H_2 in the pumping train. The trap permits high conductance (under typical operating conditions, the pressure drop across the trap is only a few percent) and high trapping efficiency. The trap structure consists of a series of alternating warm and cold fins (warm fins on the outside and cold fins on the inside) to counter the effects of "snow" formation and entrainment, which has been observed in other UF_6 traps. "Snow" formed in the gas moving through the trap should be evaporated on the outer warm fins, and the UF_6 subsequently deposited on the inner cold ones.

The nozzle source is made of high-purity nickel in order to resist UF_6 corrosion, and is heated by a 500-W cartridge heater. To insure good temperature equilibrium, the gas follows a helical path around the cartridge heater, but does not come in contact with it. The UF_6-carrier gas mixture is only in contact with high-purity nickel at high temperatures, and with ordinary nickel or monel, at temperatures below 100 °C. The source was tested at temperatures up to 300 °C and 15 atm with UF_6-He mixtures. The nozzle aperture (0.025 cm) is in a small end cap, which facilitates the changing of aperture sizes or replacement if plugging occurs. The entire nozzle assembly is supported from a series of slide assemblies located atop Stage I. The latter permit motion in three orthogonal directions for beam-alignment purposes. The position of the nozzle assembly is shown in Fig. 2. The skimmer (Beam Dynamics, Inc., Minneapolis, Minn. made by electrodeposition of nickel onto a preformed conical mandrel, was typically 0.05–0.1 cm in diameter.

In order to form the proper gas mixture for expansion out of the nozzle, the UF_6 (or other seed species) must be added to the carrier gas (either He or H_2) at relatively low concentration. For permanent gases with sufficiently high vapor pressures (such as SF_6), the gas is simply injected directly into the flowing carrier gas through an appropriate

leak valve. For liquid or solid substances, however, the seeding was effected by means of a mixing cell. The mixing cell, a 35-cm-long and 20-cm-diam monel cylinder, was originally designed for use with liquids. A portion of the carrier gas enters the mixing cell at the base of one end and flows into a 30-cm-long tube, along which sixty 0.08-cm-diam holes have been drilled. The carrier gas bubbles through the liquid, entraining seed molecules, and then exits the mixing cell through a metal mesh filter (to remove entrained droplets). A separate port on the top of the cell allows for rapid filling of the mixing cell. The cell can be warmed by heating tapes, as well as by ring heaters on each end to increase the vapor pressure of the seed material or, in the case of UF_6, to melt the solid UF_6. Most of the carrier gas can be bypassed around the mixing cell, and thus control of the final concentration of seed material is effected by adjusting the fraction of carrier gas allowed to pass through the mixing cell.

Experiments demonstrated that effective seeding of UF_6 could be accomplished *without* melting the solid hexafluoride. Apparently, the UF_6 evaporation rate from the solid phase (its vapor pressure at room temperature is ~ 100 Torr) is sufficient to provide adequate vapor pressure for seeding. The seed concentration was calculated from measurements of the reduction of the carrier gas flow on passage through the mixing cell. Downstream of the mixing region the gas mixture passed through a 2-liter buffer cell, which was necessary to damp out oscillations in the beam intensity caused by coupling between the nozzle flow and the seeding process. Under certain flow conditions, this coupling caused large, rapid oscillations in the UF_6 beam intensity. After installation of the buffer cell, no further oscillations were observed. With the above system and a temperature of the mixing cell between 30 and 45 °C, a very stable UF_6-carrier gas mixture could be formed over a wide concentration range.

B. Stage II

Stage II provides a buffer chamber which isolates the high pressure of Stage I from the quadrupole mass filter in Stage III. It also allows final collimation of the UF_6 beam before it enters Stage III, and serves as a convenient place for a beam chopper to effect beam modulation.

The construction of Stage II can be seen in Fig. 2. The width of the chamber along the beam axis is very small in order to minimize the distance between the nozzle and the quadrupole mass filter. In order to insure adequate pumping, large cylinders were welded at the top, bottom, and one side of the chamber, these latter leading to a 10-in. oil-diffusion pump. This arrangement provides virtually the maximum possible pumping speed for such a configuration. The diffusion pump is protected from UF_6 by two 10-in. liquid-N_2 baffles in series, which can be isolated from the diffusion pump by a 10-in. valve. A slide valve on the downstream wall of Stage II permits vacuum-tight isolation of the Stages I and II systems from the quadrupole mass filter in Stage III.

C. Stage III

Stage III contains four functional units: (1) the Cs atom source used in the formation of the Cs^+-UF_6^- plasma; (2) the quadrupole mass filter; (3) liquid-N_2-cooled baffles surrounding the QMF to collect material ejected from it; and (4) lenses to extract ions from the QMF and to focus them onto associated collection plates. (See Fig. 2 for a layout of the Stage III components.)

The Stage III chamber is constructed as a monel frame with removable aluminum plates on four of the faces (top, bottom, and two sides). The use of monel for the frame provides the necessary strength as well as good corrosion resistance to both UF_6 and the alkali metals. The upstream side of Stage III is covered by the Stage II wall. To prevent corrosive attack of CsOH (formed on venting Stage III) on the aluminum wall of Stage II, a thin stainless-steel plate is mounted across the upstream side of Stage III. A 6-cm-diam hole on the beam axis permits the UF_6 to pass into Stage III. On the downstream side of Stage III, a 3.5-cm-thick aluminum bulkhead serves to isolate Stage III from Stage IV. The bulkhead has a 10-cm-diam opening on the beam axis, fitted with a vacuum-tight slide valve. The chamber [128 cm long, 122 cm wide, and 66 cm in height (inside dimensions)] is evacuated by a pumping station similar to that of Stage II.

The alkali source was designed specifically for use with Cs. Although Cs is the most reactive alkali metal from the point of view of deleterious side reactions, it is also the most easily ionized, and its use insures the formation of the ion-pair plasma at moderate energies of the accelerated UF_6. The Cs source provides a well-collimated, intense beam of thermal Cs atoms which crosses the UF_6 beam either just upstream of the entrance to the QMF (referred to as crossed-beam injection) or just inside the entrance to the QMF (referred to as merged-beam injection). The two types of plasma formation will be discussed in more detail in Sec. IV C.

The Cs source is a three-stage assembly. The bulk of the Cs is held in a storage reservoir just below the vacuum system. When required, the Cs is first heated to the liquid state and then forced (by Ar pressure) up into a heated monel oven located directly under the front of the quadrupole mass fil-

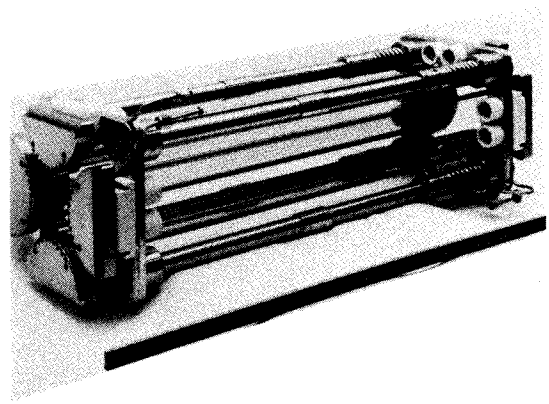

FIG. 3. Photograph of the quadrupole mass filter.

ter. The oven is heated with four cartridge heaters, and is temperature controlled. A 0.5-in. OD monel tube, henceforth referred to as the Cs source, as distinct from the Cs oven, leads from the oven to the region just upstream of the QMF. At the end of the source is a 1-mm aperture, which is located approximately 5 cm below the UF_6 beam axis. The source is heated by Thermocoax coaxial heating wire wrapped around it. The coaxial wire has an inconel outer sheath which has good corrosion resistance to both alkalis and UF_6. Surrounding the 0.5-in. monel tube is a temperature-controlled jacket (kept somewhat above the melting point of Cs), the upper end of which also serves as the final collimating orifice for the Cs beam. Cs which collects within the jacket drains down and out of the vacuum system into an external storage vessel. In the crossed-beam injection mode, the Cs beam is perpendicular to the UF_6 beam, and the Cs which traverses the UF_6 beam unreacted impinges on a beam "catcher."

The design of the quadrupole mass filter was based on several considerations. Within an ideal QMF, the electrostatic potential is given by $V = V_0(x^2 - y^2)/2r_0^2$, where x and y are rectangular coordinates measured from the axis of the mass filter (the z axis), r_0 (the field radius) is the distance from the axis to the nearest point on a pole, and $\pm V_0/2$ are the voltages on the poles. The cross sections of the poles in the x-y plane are rectangular hyperboles given by $x^2 - y^2 = \pm r_0^2$.

In an actual mass filter, the poles of necessity must represent approximations to hyperbolae, since the latter would have to be infinite in extent for a perfectly formed quadrupolar field. Cylindrical poles are frequently used in commercial QMF's because of their ease of construction. However, this approximation results in a potential which is quadrupolar only near the axis of the mass filter, and thus limits the throughput one can obtain under conditions of high resolution.

The QMF was designed for both high throughput and high resolution. As a result, a relatively large QMF having an overall length of 100 cm and a field radius $r_0 = 5$ cm was designed to insure high throughput, and the pole shape was very near a rectangular hyperbola to insure high resolution. Two other considerations are also important in the design of the mass filter: (1) the voltage required to operate the mass filter at a particular point in the stability diagram (see Paper II, Sec. II A.) increases with the square of the field radius (for a given rf frequency), and (2) the power required to operate the unit (which corresponds primarily to heat losses in the rf power supply) increases approximately with the fourth power of the field radius.[11] The chosen size of the mass filter represents a compromise between the desire for large size, the practical limitations associated with high-voltage operation, and reasonable power consumption. The power requirement of the unit constructed was approximately 1 kW.

A photograph of the QMF is shown in Fig. 3. The four poles of the mass filter are composed of stretched wires, a design previously used by von Zahn[12] and by Mosharrafa and Oskam.[13] Each pole requires 34 inconel wires (0.038 cm diam), which are supported from electrically insulated monel pole plates located at either end of the unit. Each pole plate and thus the wire structure associated with it closely approximate a hyperbola over approximately 120° of the pole surface (the angle being measured from a point $2r_0 = 10$ cm from the axis of the mass filter). The wires are spaced at 0.3175-cm intervals, so that 1 cm from the surface of the pole, the field undulations caused by the wire structure are calculated to be less than 6% of the field itself, decreasing rapidly with distance to the axis. The tension on each wire can be individually set by adjusting screws located in the end plates, so that the tension between each pair of plates (as well as on each wire) can be made approximately the same. The wire tension was determined by an acoustical technique. The use of a wire structure for the QMF has three distinct advantages. It allows for a considerable simplification in the construction of the poles; it helps significantly in the removal of ejected UF_6^- from the mass filter; and it provides for greatly enhanced pumping of the QMF.

The support structure for the mass filter consists of two monel support plates held apart by four 3.18-cm-diam monel rods. The eight pole plates are attached to the support plates, but electrically insulated from them by specially shaped ceramic (high-fired Al_2O_3) insulators. In order that the tension of the wires be held constant, the four support rods are fitted with large monel springs at one end. The rods are rigidly attached to one of the support plates, but can slide through an alignment bushing at the other support plate. The spring maintains a constant outward pressure on the pole plates, taking up any slack caused by heating of the wires during operation of the QMF.

It is particularly important that the insulators separating the grounded support plates from the pole plates be kept free from contamination. In order to insure this, the insulators are protected on the inner side by inconel metal shields located just under the wire structure (and attached to the pole plates), and on the outer side by aluminum shields which extend from the pole plate around the insulators. The latter have been removed in the photograph (Fig. 3), but can be seen in Fig. 2.

The support plates are fitted on their periphery with both cooling coils and cartridge heaters to help regulate the temperature of the unit. The radiofrequency leads are attached to the back pole plates. The whole quadrupole mass filter is supported off the base of Stage III, and surrounded by liquid-N_2-cooled baffles.

The rf power supply for the operation of the QMF, built by the ANL Electronics Division, provides two voltages: (1) a primary rf voltage V_1, which is applied in a quadrupole configuration to confine the plasma, and (2) a secondary rf voltage V_2, which is applied in a dipole configuration for mass-sensitive ejection. V_1 can be varied between 0 and 60 kV (peak-to-peak), while V_2 has a range of 0 to several hundred volts. The frequency of the ejection field ν_2 is obtained from a frequency synthesizer locked to the frequency of the confining field ν_1, which holds the frequency ratio constant to one part in 10^8.

In order to couple both voltages to the poles of the mass filter, the rf driving coil was constructed in the form of a double helix. Each helix is made of copper tubing to allow for cooling by passing air through the coil. The two coils of the helix are wound together, but insulated from one another by

encasing one coil in tygon tubing. One of the coils is capacitively coupled (near its center) to the power source of the primary voltage V_1, while the second coil is inductively coupled to the first. In order to apply the secondary rf voltage in a dipole configuration, the center taps of the two coils are connected to a power amplifier drive at the rf frequency ν_2. As a result, one end of the double helix provides two voltages, $V_1 + V_2$ and $V_1 - V_2$, while the other end provides $-V_1 + V_2$ and $-V_1 - V_2$. If these voltages are applied to the four poles of the mass filter with V_1 in a typical quadrupole configuration, then superimposed on the quadrupole field will be a dipole field directed from one pair of *adjacent* poles to the opposite pair.

Two different coils were used in the experiments which are discussed in Secs. V and VI, one producing a resonant quadrupole frequency of $\sim$0.8 MHz and the other a frequency of $\sim$0.4 MHz. The rf coil and adjustable capacitances are located in a shielded box atop Stage III. The rf lines pass through high-voltage feedthroughs and attach directly to the back end of the mass filter.

The QMF is surrounded by a pair of U-shaped Panelcoil liquid-N_2 baffles (Dean Products, Inc., Brooklyn, N.Y.), one supported from the top and the other from the bottom of Stage III. The baffles are constructed of monel, and are electropolished to provide a smooth surface to facilitate cleaning. On the pump side of Stage III, the baffles are separated by a 10-cm gap, which allows for adequate pumping of any residual He/H_2 and other noncondensable gas that enters the mass filter. On the door side, the gap between the baffles is 35 cm high, in order to permit one to install and remove the mass filter. An additional baffle to cover the gap area is mounted on the door of Stage III.

A number of extraction lenses were installed at the exit of the QMF. The lenses served to extract ions from the QMF (through the exit fringe field) and to transmit them either to collection plates mounted on the downstream wall of Stage III, or into Stage IV through the 10-cm aperture in the bulkhead separating Stage III from Stage IV. The inital set of three aluminum extraction lenses had an inner diameter of 10 cm (which is twice the field radius of the QMF itself). In experiments where the total ion throughput of the mass filter was measured, three concentric collection plates were added at the rear of the lens system, the six elements together forming a Faraday cup. This structure permitted measurements of the radial distribution of ions exiting the mass filter.

Experiments performed with the above Faraday cup demonstrated that a considerable ion flux frequently impinged on the lenses themselves, a result of the ion beam expanding greatly in the exit region of the mass filter. Consequently, a somewhat larger lens structure was constructed and used for the majority of the experiments discussed in Secs. V and VI. The latter is a four-element lens system, the first element of which is located 2.4 cm from the poles of the mass filter. The inner diameter of each lens is 15.5 cm, and their lengths are 1.25 cm for the first element and 4 cm for each of the remaining three (the separation between the lens elements is 0.8 cm). In those experiments where transmission of the ion flux into Stage IV was desired, an additional cylindrical lens was installed within the bulkhead of Stage III, so that the voltage applied to the final lens element could be maintained into the bulkhead (and up to the bulkhead slide valve). Additional ion collection assemblies were constructed for various types of experiments relating to the operation of the QMF. These elements will be described in Sec. V along with the experimental results.

D. Stage IV

Stage IV can be seen in Fig. 2, where it is attached to Stage III. The pumping station for it is similar to those for Stages II and III. In the configuration shown in Fig. 2, Stage IV was used to collect macroscopic samples of UF_6 for isotopic analysis. Details of this experimental arrangement are given in Sec. VII.

Stage IV was also used for initial tests of nozzle performance. For these tests, Stage IV was attached directly to Stage II to minimize the distance between the source and the detectors. A liquid-N_2 fin trap was installed on the back wall of Stage IV to collect the un-ionized UF_6 beam molecules which passed through the QMF and on into Stage IV. The trap has a 5-in.-diam trap area and can be isolated from Stage IV by a valve. The trap is fitted with a capacitance manometer pressure gauge, which can be used for measurements of the primary beam intensity. The condensable beam material is first collected over a period of time, the trap is then isolated from Stage IV, warmed up, and the pressure measured. From the volume of the trap and the resulting pressure, the beam flux can be determined.

The trap was particularly necessary in experiments in which macroscopic samples, corresponding to the ion throughput of the QMF in Stage III, were collected. If the collected samples are enriched (or depleted) in $^{235}UF_6$, they must not be contaminated by the un-ionized neutral beam (which is of natural abundance in ^{235}U) which exits the QMF with the ion product. However, experiments indicated that the trap was extremely efficient, and no such contamination occurred.

For measurements of the onset of UF_6 cluster formation in the Stage I nozzle, a retarding-field energy analyzer coupled with a Brink ionizer was installed in Stage IV. The molecules exiting the nozzle in Stage I, to a first approximation, all have the same velocity (which is also the velocity of the carrier gas). Thus clusters of the form $(UF_6)_n$ have energies which are approximately proportional to the cluster size and, consequently, analysis of the energy distribution of the ionized beam molecules gives direct information on the distribution of clusters in the beam without the need for separate mass analysis. The results of these experiments are given in Sec. IV A.

IV. FORMATION OF THE FLOWING ION-PAIR PLASMA

A. Composition of the plasma

The UF_6 was obtained from the gaseous diffusion plant of the Department of Energy at Portsmouth, Ohio. In order to determine its chemical purity, a sample of the vapor from the mixing cell was mass analyzed. The observed spectrum indicated the presence of only He and UF_6 in the sample (the mixing cell was at 2 atm He pressure).

Ideally, the UF_6 beam should be composed only of UF_6 monomers, with a negligible fraction of the polymeric species $(UF_6)_n$. This results in an ion-pair plasma that contains only Cs^+ and UF_6^- ions in their natural isotopic ratios, and thus simplifies the theoretical modeling of the system, as well as the interpretation of the experimental results.

To determine nozzle conditions which give the desired beam composition, diagnostic measurements on the UF_6 beam were made to obtain its polymer content as a function of both the UF_6 concentration in the nozzle as well as the nozzle pressure. In these experiments, Stage IV was attached to Stage II. A Brink ionizer was used to ionize the UF_6, and a retarding-field energy analyzer enabled us to indentify separately the lower molecular-weight polymers present in the UF_6 beam.

With $\sim 1\%$ UF_6 in He at 2 atm nozzle pressure and 150 °C nozzle temperature, the monomer/dimer/trimer/tetramer signals from the retarding field energy analysis were in the ratios 27:15:5:2. If we assume that the ionization efficiency of the dimer is approximately twice that of the monomer, and correspondingly higher for the higher polymers, the beam composition at 1% UF_6 in He was approximately 75% monomer and 25% polymer. At concentrations of $\sim 0.1\%$, only the monomer was observed, although poor statistics do not preclude a small fraction of polymers in the beam at this concentration. The final operating conditions for the bulk of the experiments discussed in this report were chosen to be 0.3% UF_6 in He at 2 atm pressure and 150 °C nozzle temperature. Under these conditions, we believe the composition of the beam is predominantly monomer, with relatively small concentrations of dimer and higher polymers. At higher nozzle pressures, polymerization increases greatly, and higher nozzle temperatures are prohibited because of rapid plugging of the nozzle. No further measurements of polymer content were made after the carrier gas was changed from He to H_2. Concentrations of UF_6 in H_2 were 0.5% or less.

Measurements of the ionic composition of the plasma were initiated to search specifically for F^-, as a result of an extraneous resonance that appeared in the operation of the QMF (see Fig. 14). In these experiments, a chamber in the form of a cross was attached to the downstream side of Stage III, at the exit aperture of the QMF, and an analytical quadrupole mass spectrometer (Extranuclear Laboratories, Pittsburgh, Pa.) was mounted on the cross at 90° to the UF_6 beam axis. The ions exiting Stage III were deflected into the analytical QMF by a pair of deflection grids, while the unreacted UF_6 impinged on a liquid-N_2 fin trap attached to the downstream side of the cross.

The only dominant ions observed in the mass spectrum were Cs^+ and UF_6^-. No F^- or F_2^- were found, the F^-/UF_6^- ratio being less than 10^{-7}. The UF_5^-/UF_6^- ratio was approximately 1/500. Cs_2^+ dimer was also observed, with a Cs_2^+/Cs^+ ratio of approximately 1/500, suggesting that the UF_5^- might be formed by reaction of UF_6 with Cs_2 dimer. Polymeric ions of UF_6 could not be searched for, owing to limitations in the mass range of the analytical mass spectrometer.

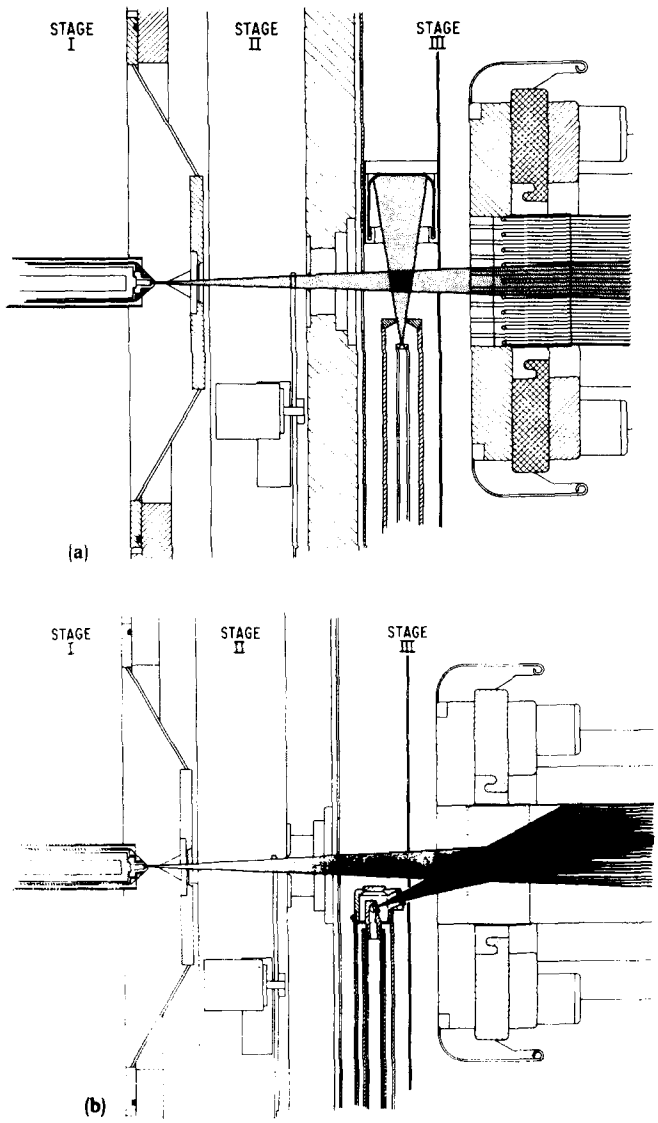

FIG. 4. (a) Scaled drawing of the arrangement for crossed-beam formation and injection of the ion-pair plasma into the quadrupole mass filter. (b) Scaled drawing of the arrangement for merged-beam formation of the ion-pair plasma within the quadrupole mass filter.

The presence or absence of polymeric UF_6^- ions in the plasma can be inferred from the behavior of the UF_6^- resonance in the presence of combined quadrupole and dipole fields in the Stage III mass filter (see Sec. VI for a complete discussion of the resonance behavior). As the dipole field strength was increased at the UF_6^- resonance, the UF_6^- ion signal (representing the throughput of the QMF) decreased, as more and more UF_6^- was ejected from the mass filter. Since this ion signal could, in fact, be reduced virtually to zero with a moderate dipole field strength, the plasma must be relatively free of polymeric ions, since these ions would be in stable trajectories at the UF_6^- resonance, and thus constitute an irreducible ion signal.

B. Plasma density

As a result of the collision of the Cs and UF_6 beams, a flowing ion-pair plasma was formed which travels toward

the entrance of the QMF. Actually, the flowing plasma moved along the direction of the center-of-mass motion of the UF_6-Cs collision system. Since the UF_6 molecule was moving initially along the axis of the QMF with a kinetic energy of ~ 6.8 eV for UF_6 accelerated in He or ~ 10.6 eV for UF_6 accelerated in H_2 (both energies corresponding to 150 °C nozzle temperature), and since the Cs was moving vertically with a kinetic energy of ~ 0.075 eV (corresponding to 300 °C source temperature), the center-of-mass motion was inclined from the QMF axis by $\theta = \tan^{-1}(v_{Cs}/v_{UF_6}) = 9.7°$ for the He carrier and 7.8° for H_2. Once within the influence of the QMF, however, this slight vertical motion is generally small compared to the velocities induced by fields of the mass filter itself, although such off-axis motion does have some effect on the mass resolution of the unit.

The density of the plasma can be obtained from the relation $F = nvA$, where F is the ion flux (positive or negative) in ions/sec, v is the velocity of the flowing plasma (i.e., the velocity of the center-of-mass motion), n is the density of the positive or negative ions, and A is the cross-sectional area of the plasma. The velocity can be estimated from the nozzle conditions, and the ion flux is measured directly. In the latter measurement, the poles of the QMF itself were used to collect the ion flux. The upper pole was biased at a negative potential relative to the remaining poles when measuring the positive ion flux, and conversely for negative ions. From this measurement and an estimate of the area A, the density of the plasma in the region where it is formed could be determined.

At the highest Cs fluxes, a UF_6^- ion current of 1.2×10^{-4} A was obtained on the pole of the mass filter, for UF_6 accelerated in He (the ion current was a linear function of the Cs pressure in the source over the entire pressure range measured, i.e., 0.1–15 Torr). With a UF_6 velocity of 1.40×10^5 cm/sec (corresponding to a 6.8-eV UF_6 beam energy) and an area $A = 2.21$ cm^2, the maximum plasma density was therefore 3.3×10^9 ions/cm^3. When He was replaced by H_2 to produce a higher energy UF_6 beam, a factor of 4 increase in the measured negative ion flux was obtained, which corresponds to a peak plasma density of 1.1×10^{10} ions/cm^3, taking into account the higher UF_6 velocity obtained with the H_2 carrier gas.

The electron-transfer cross section for the reaction $Cs + UF_6 \rightarrow Cs^+ + UF_6^-$ can be estimated from the above measurements in conjuction with a determination of the two neutral beam intensities. The UF_6 beam flux was determined by collection of the beam on the Stage IV liquid-N_2 fin trap (see Sec. III D.) and corresponded to a flux of 4.90×10^{16} molecules/sec for UF_6 accelerated in H_2. The density of the Cs beam was estimated from the vapor pressure of the Cs in the oven and the temperature of the Cs source. From the beam intensities, the ion flux, and the interaction volume of the two beams, a charge-transfer cross section of 174×10^{-16} cm^2 was obtained at a relative energy of 2.91 eV. The uncertainty in the cross section is estimated to be about a factor of 2. The electron-transfer cross section measured here appears to connect in a reasonable way to the measurements of Annis and Datz[9] at lower collision energies.

At the highest Cs beam intensities, a measured UF_6^- ion current of 4.8×10^{-4} A and a measured flux of neutral UF_6 molecules of 4.9×10^{16} sec^{-1} implies a maximum ionization efficiency of 6.1%. Thus at the maximum throughput, the neutral UF_6 density is ~ 16 times greater than the ion density (the latter being $\sim 1.1\times 10^{10}$ ions cm^3). One can easily show that at these density levels, ion-ion and ion-neutral collisions are negligible during the transit time of the UF_6^- through the QMF (~ 1 msec). Thus the plasma can be considered collision-free. For the same reasons, two- or three-body ion recombination within the QMF can be neglected.

C. Plasma injection

The initial design of the apparatus called for the formation of the ion-pair plasma in the region centered 5-cm upstream of the QMF, permitting the plasma to drift into the mass filter itself (crossed-beam injection). This method of injection is shown in Fig. 4(a). Since the plasma is electrically neutral, electric fields cannot be used to speed up or slow down the axial motion of the moving plasma. Such fields would only pull apart the plasma into its positive and negative components. A grounded plate was installed between the Cs source and the QMF, the plate having a 2.5-cm-diam hole centered on the UF_6 beam axis, through which the plasma passed subsequent to its formation. The grounded plate served to keep the QMF free from extraneous Cs vapor, and thus reduce arcing problems, and to isolate the region of formation of the plasma from the fringe field of the QMF.

As demonstrated below, this method of plasma injection proved ineffective when the rf voltage on the mass filter was increased to high levels. Extensive experimentation (see Sec. V) suggested that only a small fraction of the plasma was entering the mass filter at high rf voltages, a difficulty traced to the fringe field of the mass filter. For ions moving off the axis of the QMF, the fringe field produces axial forces which reflect back upstream a substantial fraction of the ions that were initially moving toward the entrance of the mass filter. Although the grounded plate described above isolates the region of formation of the plasma from the fringe field, the plasma must ultimately pass through the fringe field.

To eliminate the deleterious effect of the fringe field, a merged-beam technique was employed to form the plasma within the QMF itself (actually from ~ 1 cm out of to ~ 5 cm within). The Cs source was redesigned to produce a Cs beam which passes through a hole in the grounded plate, and then crosses the UF_6 beam within the QMF. The bulk of the Cs then passes through the wires of the mass filter, and impinges on the liquid-N_2 baffle above it. The actual arrangement is shown in Fig. 4(b). Although in this mode the Cs passed directly through the wires of the mass filter, its density there was sufficiently low so that no arcing problems were encountered. (The upper wire structure near the front of the mass filter did accumulate a deposit of Cs after long-term operation, although no specific detrimental effects associated with these deposits were observed.) By this method of plasma formation, the effect of the fringe field at the front of the QMF was effectively eliminated. However, it should be emphasized that the plasma must still pass through the exit fringe field in order to leave the mass filter. This will be discussed in Sec. V.

V. PLASMA CONFINEMENT AND TRANSMISSION IN QUADRUPOLE FIELDS

In the high-flux regime, the behavior of a beam of ions, all of the *same* charge sign, in the QMF of Stage III would be dominated by space-charge forces. These repulsive Coulombic forces present within the dense input ion beam can overpower any realistic applied confining field, and cause the beam to blow up radially. The expansion continues until the ion density within the mass filter decreases to sufficiently low values that the applied quadrupole field is comparable to the space-charge forces. In our experiments, however, the input beam is an electrically neutral, flowing ion-pair plasma, and hence the behavior of the plasma in the QMF will not be directly limited by space-charge blowup. Instead, the behavior will vary between two extremes according to density. At very low densities, the ions will not interact with one another, and the mass filter will operate on the plasma as it does on any low-density ion flux. On the other hand, at very high densities, the plasma shields itself from the applied fields, and therefore cannot be readily manipulated. However, at intermediate densities, applied fields can penetrate the plasma, which moderates its response by its tendency to preserve charge neutrality.

In this section, the experimental results for confinement and transmission of the plasma through the QMF will be presented. In these experiments, only a quadrupole field is applied to the mass filter in an attempt to confine the plasma within it. The isotopic selectivity of the QMF involves *ejection* of certain mass components of the plasma, and involves the simultaneous application of both quadrupole and dipole fields. Discussion of this process is deferred until the next section.

In Sec. II A. of Paper II,[2] the well-developed theory of low-density ion motion in a QMF will be briefly reviewed and applied to our experimental conditions. It is recommended that this section be read before proceeding to the experimental results below. The theoretical treatment of the motion of a high-density plasma in a QMF is considered in Paper II, Sec. III,[2] which also includes a comparison of the theoretical and experimental results.

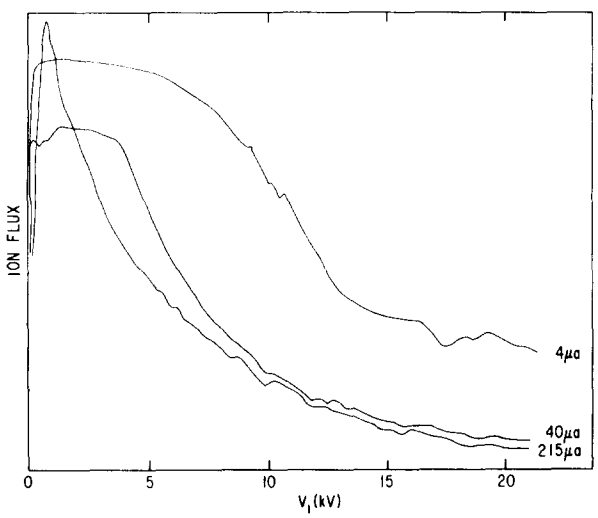

FIG. 5. UF_6^- confinement curves for three different input fluxes, with use of the crossed-beam injection mode and He as the carrier gas.

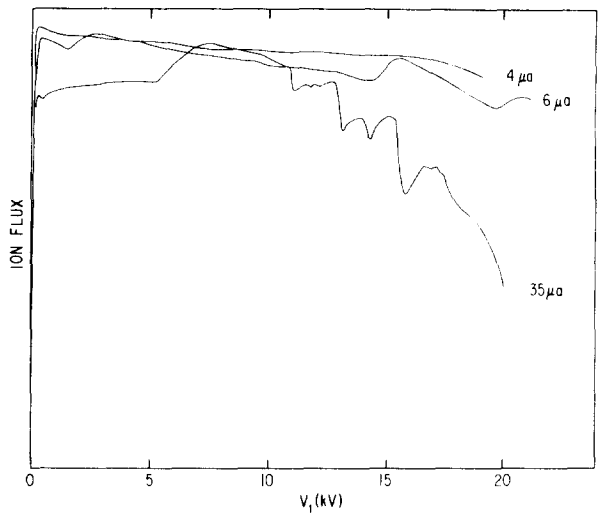

FIG. 6. UF_6^- confinement curves for three different input fluxes, with use of the merged-beam injection mode and He as the carrier gas.

Experimental results relate to the following three areas: (1) injection of the plasma into the QMF through the entrance fringe field, (2) problems associated with measuring the ion throughput of the mass filter, and (3) the degree of confinement within the mass filter itself. We will consider first experimental results corresponding to an rf quadrupole field with $\nu_1 = 0.8$ MHz. At this frequency, both the Cs^+ and UF_6^- are within the stability diagram in the low-density limit, and should be confined within the mass filter for a quadrupole voltage V_1 from a few hundred volts to ~ 40 kV.Our basic measurement involves determining the *confinement curve*, i.e., the positive or negative ion throughput of the mass filter as a function of V_1, for various methods of plasma injection and for various methods of extracting the plasma from the exit of the mass filter. Confinement curves were generally determined from 0 to ~ 20 kV, above which arcing within the mass filter was frequently encountered. Clearly, at 0.8 MHz and sufficiently low plasma density, the confinement curves for Cs^+ or UF_6^- should be flat from the onset of confinement at a few hundred volts to 20 kV.

The voltage V_1 indicated in the following figures is the rf peak-to-peak voltage determined from a pickup coil located near the main rf driving coil for the QMF. Calibration of the system indicated some nonlinearity in the ratio of the pickup coil voltage to the actual measured voltage on the poles of the mass filter, especially in the range $0 < V_1 < 1$ kV. The V_1 scale in the following figures is correct at 8 kV, and is in error by no more than 4% over the range 5–20 kV, the actual voltage being slightly lower than indicated for $V_1 > 8$ kV and slightly higher for $V_1 < 8$ kV.

In Fig. 5 we give experimentally recorded confinement curves for UF_6^- at three different input fluxes for the crossed-beam injection mode, which corresponded to estimated initial UF_6^- ion densities of 1.1×10^8, 1.1×10^9, and 5.9×10^9 cm^{-3}. These initial densities gave observed peak

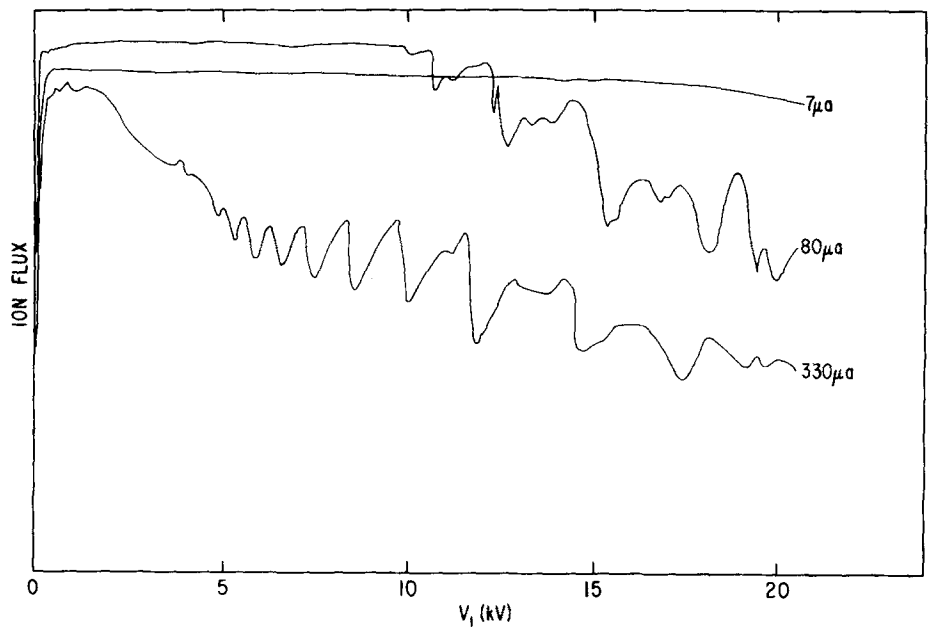

FIG. 7. UF_6^- confinement curves for three different input fluxes, with use of the merged-beam injection mode and H_2 as the carrier gas.

ion currents of 4, 40, and 215 μA, respectively, which are so labeled in the figure. The initial density of UF_6^- ions was determined (see Sec. IV B.) from the UF_6^- flux, the area of the UF_6 beam at the position of the Cs cross beam, and the velocity of the UF_6. The recorded signal is the output current of the QMF measured by a detector composed of four cylindrical lenses and a back plate all centered about the quadrupole axis, with the back plate located about 20 cm from the exit of the mass filter. The lenses and plate were set at + 200 V, making the detection system in effect a Faraday cup. The curves are *not* on the same scale, but each curve is labeled by the current at its peak. Clearly, the confinement curve is not flat from a few hundred volts to 20 kV, but drops off to a degree that increases with increasing input flux. Confinement curves for Cs^+ show the same effects. The similar output currents for ions of opposite charge sign were typical of all experiments with $\nu_1 = 0.8$ MHz.

In Fig. 6, we give confinement curves for UF_6^- in the merged-beam configuration. For this experiment, two cylindrical lenses and the back plate were the detection system; all elements were set to + 200 V, again making it in effect a Faraday cup. Note that the drop-off is much less severe than in the crossed-beam geometry, especially at the lower peak current of 4 μA. In this and the previous experiment, the carrier gas used in the aerodynamic acceleration of UF_6 was He. As discussed earlier, when H_2 is substituted for He, its

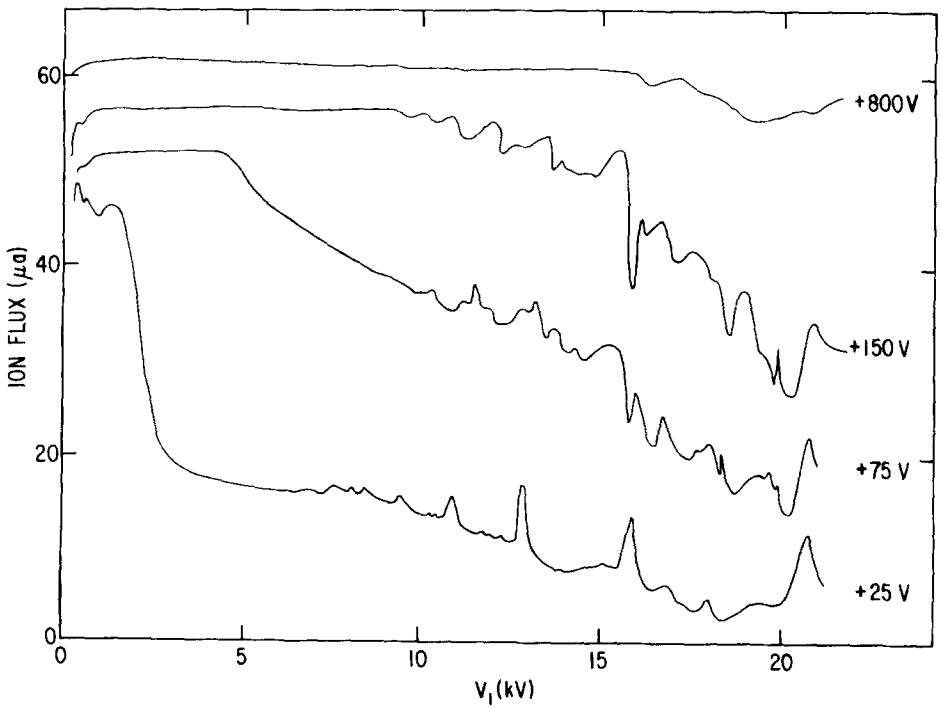

FIG. 8. UF_6^- confinement curves as a function of the extraction-detection voltage for a constant input flux. H_2 was the carrier gas, and the merged-beam injection mode was used.

lighter mass results in a more highly accelerated UF_6 by about 4 eV of kinetic energy ($\sim$10.6 eV vs $\sim$6.8 eV). This additional energy would be expected to improve the ability of the ions to overcome any fringe-field effects. In Fig. 7 are recorded confinement curves for UF_6^- in the merged-beam configuration with H_2 as the carrier gas. The detection system was the same as in the previous experiment. The falloff of the confinement curve is significantly improved over that for the He carrier, but still grows worse with increasing throughput. The falloff is also characterized by oscillations which grow more pronounced at higher values of V_1 and higher ion throughput.

The strong influence of the mode of plasma injection and the kinetic energy of the flowing plasma on the observed confinement curves are manifestations of the problem of transporting a plasma with little axial kinetic energy across the fringe field at the entrance of the mass filter. As discussed in greater detail in Paper II, Sec. IV, this fringe field, although primarily transverse, has an axial component that grows in strength with increasing V_1 and with increasing radial distance from the axis. These axial forces can have two interrelated effects. First, axial fields will reflect ions of low axial energy that are sufficiently radially displaced from the QMF axis. Second, both axial and radial components of the fringe field induce plasma disruption and consequent space-charge blowup. While the radial field is designed to confine ions, the axial field reflects ions with greater efficiency the more the plasma expands. Model calculations of the fringe field and of ion motion in the fringe field demonstrate considerable reflection of the plasma at higher values of V_1 and at higher plasma densities. This is in accord with the measurements just presented. Forming the plasma within the mass filter (merged-beam injection) considerably reduces the entrance fringe-field problem, although it is not entirely eliminated since fringing persists to about one field radius into the QMF.

At the exit of the QMF, the plasma encounters a second fringe field, with similar effects. Furthermore, in addition to the fringe field, there is an applied field for the extraction and collection of ions of one charge sign from the plasma. The extraction fields must destroy the plasma, since they are biased to collect ions of only one charge sign. The axial components of these fields have the same effect as the axial fringe fields, insofar as they participate in the plasma blowup and the reflection of ions. Together these fields can substantially affect the collection of ions at the collector plate.

Evidence of collecting effects can be found in the observed oscillations shown in Figs. 7 and 8. These oscillations are sensitive to the voltage of the detection system, as shown in Fig.8. Here, four recorded confinement curves are shown, all on the same current scale, for merged-beam plasma injection with H_2 as the carrier gas. Again, two cylindrical lenses and a back plate were used to measure the output current of the mass filter, the voltage on the three-element detector being indicated in the figure for each curve. Note that the oscillations flatten out and the detected current increases as the detector voltage increases. Since for merged-beam plasma injection the input-ion flux depends only weakly on V_1, the observed oscillations and falloff in the confinement curve at high V_1 most likely reflect the problem of extracting ions through the exit fringe field. As the detector voltage increases, the predominantly axial extraction field overrides the axial QMF fringe field for all but the highest values of V_1, producing the flatter confinement curves of Fig. 8, and essentially 100% transmission of the ion flux.

Direct evidence of ion-reflection effects can be seen in the Cs deposits which build up on the *downstream* side of the plate between the Cs source and the mass filter [see Figs. 4(a) and (b)]. These deposits shadow the front support structure of the mass filter. This indicates that Cs^+ ions stream toward the entrance of the mass filter from a source near its exit, i.e., the fringe-, extraction-, and collection-field region during UF_6^- collection. The detection system in operation during the Cs deposition was a Faraday cup whose axially dominant fields enhance UF_6^- collection, as seen in Fig. 8, while reflecting all the transmitted Cs^+. Because the fringe fields at either end of the QMF can reflect the Cs^+, Cs^+ may make several passes through the QMF before making the observed deposits or being deflected elsewhere.

The reflection of ions of only one charge sign back into the QMF by an extraction and collection system produces excess charge within the QMF. At high enough density, this excess charge could severely affect the plasma and its confinement. In order to assess the importance of reflecting ions upsteam through the mass filter, an ion-collection system was constructed consisting of a pair of top and bottom hemicylindrical plates that could be separately biased at a positive-negative potential, leaving the axis of the mass filter at zero potential. By oppositely biasing the top and bottom half-cylinders, it was hoped that the plasma could be pulled apart radially, thus minimizing the streaming of oppositely charged ions back into the mass filter, as appears to happen with a Faraday cup arrangement. The results for crossed-beam injection, and hemicylinders biased at $\pm$500 V, showed no substantial improvement in the confinement curve over that with Faraday cup collection. Surprisingly, the flux of either ion collected on the top half-cylinder was always somewhat larger than that on the bottom half-cylinder. Prior to this experiment, the entire apparatus had been carefully aligned. In fact, deliberate and accidental misalignment changed but did not qualitatively affect this lack of symmetry in the collected current. The only source of asymmetry is a grounded asymmetric baffle and support structure at the end of the QMF, but rather far removed from the axis of the mass filter.

Besides the disruptive effect of reflected ions, the field of the extraction system can exert an additional influence on the operation of the mass filter. Since the plasma is a conducting medium, it was thought that the bias of the detection system may be conducted by the plasma through the mass filter and into the region of plasma formation. Strong fields generated in this region would tend to tear the plasma apart, and thus possibly effect the falloff in the confinement curves. In order to test this hypothesis, a grounded grid was placed over the entrance hole of the large grounded plate separating the Cs source from the mass filter, through which the plasma passes before entering the mass filter [in the crossed-beam injection mode; see Fig. 4(a)]. In addition, grids were placed

over the second and third cylindrical lenses in a detection system composed of four cylindrical lenses and an end plate. The first lens as well as the grid on the second lens were grounded, essentially isolating the mass filter from the externally applied fields. The grid on the third lens permitted retarding-energy analysis to be performed on the ions which flow through the grid on the second lens.

In Fig. 9 confinement curves are shown for various voltages on the third cylindrical lens, with the first and second lenses grounded. The curves are for crossed-beam injection with He as the carrier gas. The UF_6^- was collected on the fourth cylindrical lens and the back plate, both at a voltage of + 100 V. The flux for the third lens voltage at + 100 V appears to have become almost saturated, implying that above this voltage all the ions which pass through the first grid on the second cylindrical lens are subsequently collected on the collector. The upper two curves in Fig. 9 show that the grounded grids fore and aft of the mass filter do not influence the decline of the confinement curve at high values of V_1, since the falloff is similar to that observed without the grids. This is in agreement with earlier discussion which concluded that the difficulty of plasma injection was the cause of the nonflat confinement curve.

An additional characteristic of extraction and detection that was observed in *all* experiments was the lack of saturation of the detected signal with increasing extraction voltage. The peak current of the confinement curve increased slowly but continuously as the voltage on the Faraday cup was increased, the input conditions remaining constant. The same effect occurred at low or high throughput, for all injection and extraction-detection systems, and for both positive and negative ions. The lack of oscillations in the confinement curves at the lower values of V_1 suggests that the failure to saturate is not directly related to the exit fringe field. The origin of the increasing ion signal is unclear.

In conclusion, no specific detrimental effects of the extraction voltage on confinement of the flowing ion-pair plasma by the QMF were demonstrated in our experimental studies. The extraction geometry and voltages mainly influence the transport of the ion beam across the exit fringe field, but do not severely affect ion motion within the mass filter itself. This conclusion, however, may not be valid at higher throughput.

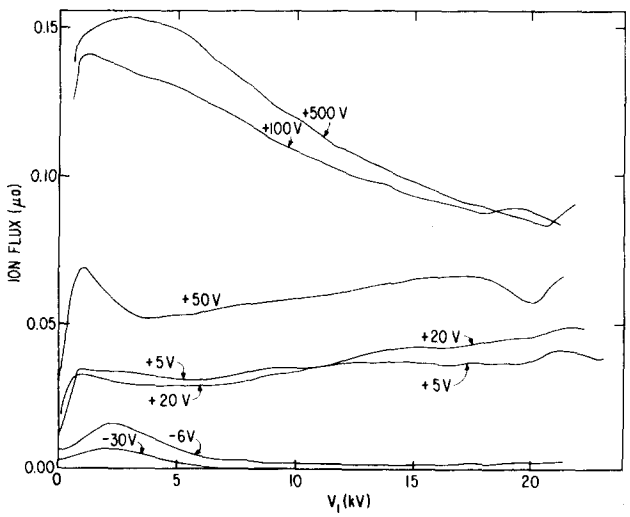

FIG. 9. UF_6^- confinement curves as a function of the extraction voltage downstream of two grounded grids which isolate the mass filter from the extraction-detection system.

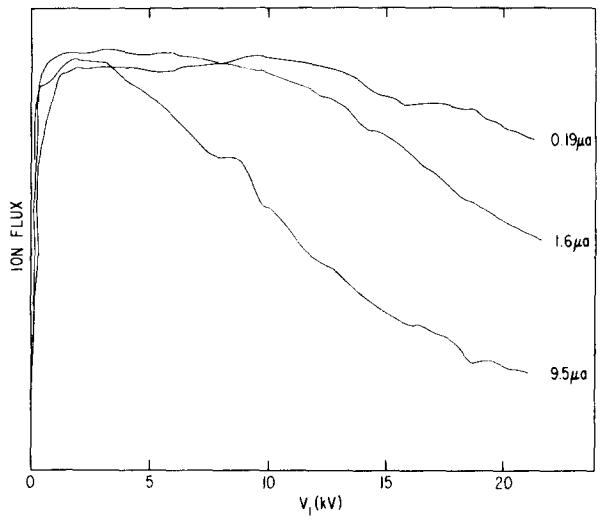

FIG. 10. UF_6^- confinement curves for three different input fluxes, with use of the 2-mm-diam collimator aperture. These curves should be compared with those of Fig. 5, where a 10-mm-diam aperture was used.

Direct evidence for efficient confinement of the plasma within the QMF was obtained by measurements of the loss of UF_6^- flux through one pole of the mass filter as a function of V_1. The detector here was a series of plates parallel to the axis, but located just outside the pole structure. Above $V_1 \sim 7$ kV, no signal was recorded by the array of plates for peak transmitted UF_6^- fluxes up to 8 μA, the highest flux used in this experiment. This experiment demonstrates that, for a sufficiently high quadrupole voltage, the confinement of the plasma at this flux level can be made complete, despite space-charge forces which are already quite significant (see Paper II, Sec. III for the onset of measurable space-charge effects).

Additional experiments were made to determine the dependence of the confinement curve on the initial cross-sectional area of the plasma, as controlled by the diameter of the UF_6 beam collimator located on the downstream wall of Stage II. In Fig. 5, a 10-mm-diam collimator was used, implying, by straight-line trajectories, an initial circular plasma size of 1.0–1.5 cm radius at the entrance to the mass filter. Entrance fringe fields will distort the actual trajectories from straight-line paths, making the 1.5-cm radius estimate only a rough guide.

In Fig. 10, results for a 2-mm-diam collimator are displayed. The extraction-detection system was a series of cylindrical lenses and back plate operated as a Faraday cup at + 100 V. Comparison of the results in Figs. 5 and 10 shows that the initial size of the distribution has little influence on the shape of the confinement curve at a given peak output current. This result seems at first surprising, since a flowing plasma of larger radial extent encounters stronger axial

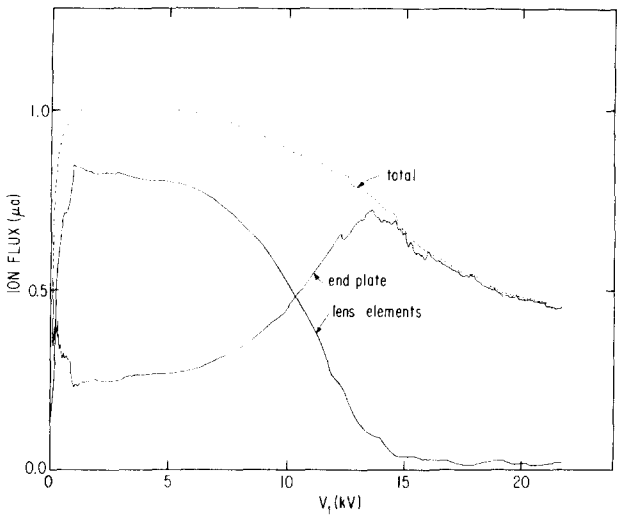

FIG. 11. UF_6^- confinement curves as determined from the ion flux collected by the end plate, by the cylindrical lens elements, and by all elements of the Faraday cup, respectively.

fringe fields on entering the QMF. However, at the same input flux a radially condensed plasma is much more dense, and is thus subject to stronger space-charge forces upon disruption by the fringe fields. The experimental measurements in Figs. 5 and 10 indicate these two effects operate to minimize the effect of the initial cross-sectional area of the plasma. (For a more complete discussion, see Paper II, Secs. III and IV.[2]) In the merged-beam plasma injection method, the effect of plasma size on confinement is expected to be minimal. However, it was not measured.

Until now we have discussed measurements of the total ion throughput of the QMF. In order to collect macroscopic samples, however, the ion throughput must be transported into Stage IV via the 10-cm-diam port in the bulkhead separating Stages III and IV. The following measurements were concerned with determining the extraction conditions at the exit of the mass filter that maximize the fraction of ions transported into Stage IV.

In Fig. 11, we decompose the UF_6^- confinement curve measured by a Faraday cup into the portion measured by the four cylindrical lenses and the portion measured by the back plate, all elements biased at + 100 V. The injection method was crossed beam, with the consequence that the total confinement curve falls off at high V_I, but this is not pertinent to the present discussion. The figure demonstrates an effect that was commonly observed with the Faraday cup ion-collection geometry. At low quadrupole voltages a portion of the ion flux appears on the cylindrical lenses, but on raising V_I the ion flux moves almost entirely to the end plate. The fraction of ion flux appearing on the cylindrical lenses at low V_I decreases with decreasing throughput in the mass filter, and at a throughput somewhat lower than that shown in Fig. 11, the ion flux was entirely collected on the end plate for all V_I.

These observations can be explained in the following way. The collection of ions of one charge sign at the exit of the mass filter by axially dominant collection fields destroys the neutral plasma by reflecting ions of the opposite charge back upstream through the mass filter. The remaining ion beam, accelerating toward the Faraday cup, will tend to blow up by space-charge repulsion, the blowup increasing with increasing ion density. At the same time, the rf fringe field at the exit of the mass filter, which increases with V_I, will tend to counter the blowup, and keep the ions localized near the axis (although some reflection of the UF_6^- ions can also occur). Since only a relatively small quadrupole voltage is sufficient to confine the ion beam in the absence of space-charge forces, the fringe field can have a substantial effect over a considerable distance into the extraction region. Thus, the radial distribution of ions that appear at the collection elements results from a balance between the space-charge blowup of the ion beam and the confining force of the fringe field. At low V_I in Fig. 11, the space-charge blowup

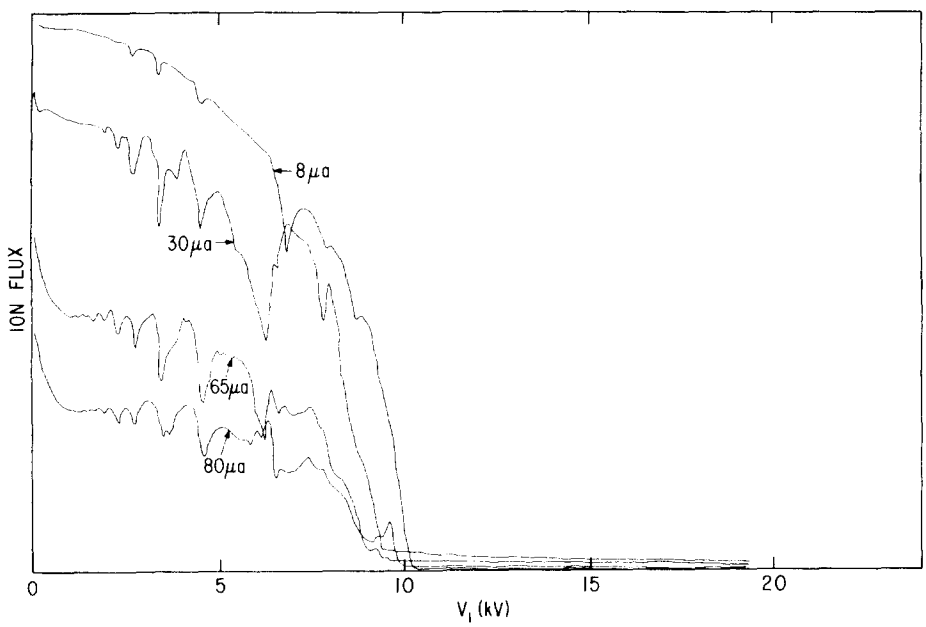

FIG. 12. Cs^+ confinement curves for several peak output fluxes at $\nu_I \simeq 0.4$ MHz, and the crossed-beam mode of plasma injection.

forces the majority of the ion flux to the cylindrical lenses. However, above ~15 kV, the fringe field of the mass filter is strong enough to keep the ion beam confined right up to the end plate, so that little ion flux is lost to the lenses. The space-charge blowup can also be countered by increasing the extraction voltage. This draws the ions to the end plate more rapidly, reducing the transit time during which blowup can occur, and thus decreasing the fraction of ions appearing on the cylindrical lenses.

The above effect can be seen even more clearly in an experiment in which the end plate was segmented into three concentric rings, so that the ion flux to each ring could be determined separately. This experiment was run at ~8-μA peak current, and demonstrated that at the highest quadrupole voltages measured (22 kV), 80% of the ion flux impinged on the inner two concentric rings (an area 3 cm in radius), while the remaining flux was collected on the outer ring and the fourth cylindrical lens.

From the above results at low throughput, we can anticipate the type of collection geometry that maximizes the transport of ions into Stage IV at high throughput, i.e., one that makes maximum use of the confining force of the exit fringe field with little or no extraction voltage, followed by a strong extraction field. Experimentally, the best extraction conditions for UF_6^- were obtained by removing the first two cylindrical lenses, operating with the third cylindrical lens at zero or slightly negative potential, and extracting with a high-positive voltage on the final cylindrical lens and the Stage IV lens (the elements labeled J in Fig. 2).

We now turn to experiments with $\nu_1 = 0.4$ MHz. Under these conditions, only the UF_6^- remains within the stability diagram (according to low-density theory) over the range of V_1 accessed experimentally. At $V_1 \sim 10$ kV, the Cs^+ moves out of the stability diagram, and thus above 10 kV it should not be confined by the quadrupole field in the absence of space-charge forces. The experiments performed at $\nu_1 = 0.4$ MHz were all with merged-beam plasma injection, with H_2 as the carrier gas, a 10-mm collimator, and an extraction-detection system consisting of four cylindrical lenses, two in Stage III and two in Stage IV, and a back plate downstream from the Stage IV lenses.

The confinement curves for Cs^+ and UF_6^- are shown in Figs. 12 and 13, respectively. In each case, the first cylindrical lens was grounded and the extraction current was measured to all other elements biased at 1000 V (minus for Cs^+, plus for UF_6^-). Each curve is labeled by its peak output current.

The confinement curves for Cs^+ all decreases to small values beyond 10 kV as predicted by low-density theory, and demonstrate that space-charge forces which are quite strong at the higher throughput levels (see Sec. VI) are not sufficient to *prevent* the Cs^+ from being driven out of the mass filter by the rf quadrupole field. Looked at another way, the containment of the UF_6^- beyond 10 kV, as demonstrated by the confinement curves in Fig. 13, as well as the ejection of Cs^+, illustrates the dominance of the rf quadrupole field over the space-charge forces at these flux levels. Although the UF_6^- confinement curve above 10 kV is relatively flat for the 80-μA level, theoretical calculations for similar fluxes (see Paper II, Sec. III C.)[2] show some loss of UF_6^- for $V_1 > 10$ kV, indicating only partial confinement of the UF_6^- at this flux level in the absence of space-charge neutralization.

The oscillatory behavior of the confinement curves for $V_1 < 10$ kV seen in Figs. 12 and 13 and the almost flat behavior beyond 10 kV demonstrate that the oscillations are related to the presence of the counter ion, and most likely reflect oscillating space-charge forces in the fringe field of the mass filter. The dip in the confinement curves at low V_1 (< 5 kV) at the higher throughtput is related to space-charge blowup in the extraction region, which overpowers the weak confining fringe field. The analogous effect at $V_1 = 0.8$ MHz is shown for the current to the end plate in Fig. 11. The rise in the UF_6^- throughput at ~9 kV for the 45 and 80 μA cases probably reflects the elimination of the disruptive space-charge/

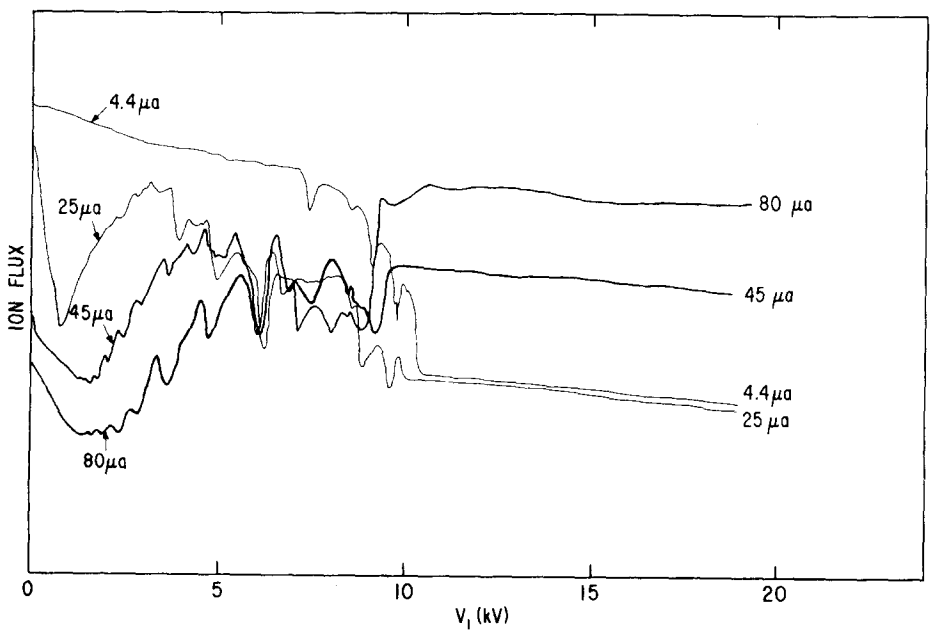

FIG. 13. UF_6^- confinement curves as a function of the peak output fluxes at $\nu_1 \simeq 0.4$ MHz, and the crossed-beam mode of plasma injection.

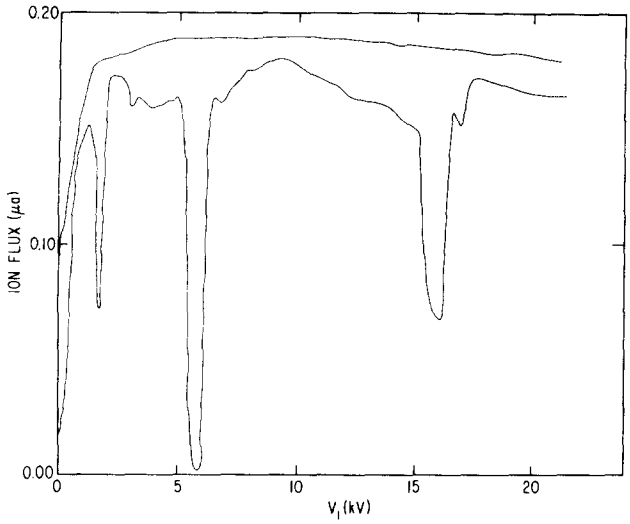

FIG. 14. Confinement and resonance curves measured for Cs^+ at ~ 0.2-μA maximum output current, with the crossed-beam mode of plasma injection.

fringe-field interaction subsequent to driving out the Cs^+. This apparently permits more efficient extraction, resulting in the sudden rise in collected current.

Increasing the bias voltage from + 1000 to 1800 V increases the confinement curve for all values of V_1, the increase at the higher values of V_1 showing the same lack of saturation of the collected current observed for the 0.8-MHz case. A larger increase at low values of $V_1 (< 5$ kV), however, reflects not only the lack of convergence, but in addition, a decrease in the space-charge blowup (and subsequent loss of ions) resulting from the more rapid extraction of the ions at high extraction voltages. Also, as was found for $\nu_1 = 0.8$ MHz, biasing the lead lens to the common bias on all the other elements does not appreciably change the curves, but does *decrease* the fraction of the detected current that strikes the back plate.

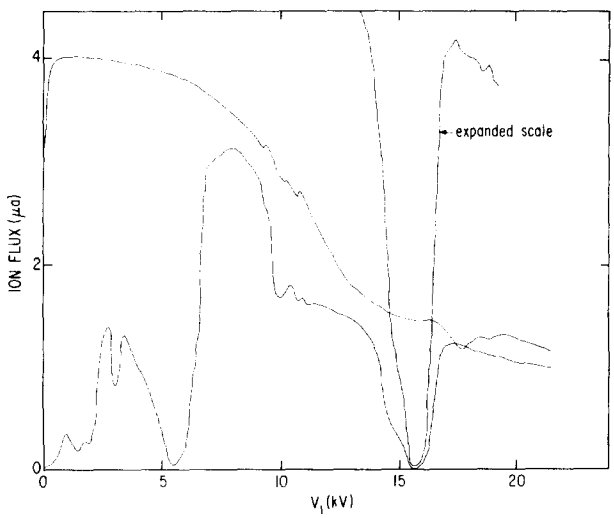

FIG. 15. Measured confinement and resonance curves for UF_6^- at relatively low-ion flux, for $\nu_1 \simeq 0.8$ MHz. The crossed-beam mode of plasma injection and a sine wave dipole field were used.

VI. ION EJECTION IN COMBINED DIPOLE-QUADRUPOLE FIELDS

In the previous section, experimentally measured confinement curves were presented which show that a substantial amount of input-ion flux can be successfully confined by a quadrupole mass filter over a wide range of the applied quadrupole voltage V_1. If an additional, nonconfining oscillatory dipole field of frequency ν_2 and amplitude V_2 is applied, low-density theory (see Paper II, Sec. V A.) shows that at resonance a weak dipole field can drive ions of a specific mass into ever-expanding orbits such that the ions eventually strike the poles of the mass filter, resulting in loss of transmission. Thus at low density, the system operates to confine all ions (within the stability diagram) except the specific one that is being ejected by the applied weak dipole field. It is the purpose of this study to demonstrate whether or not this mass-sensitive ejection can be maintained at the higher densities where space-charge forces are strongly perturbing the ion motion, i.e., to determine the resolving power of the mass filter as a function of plasma density.

In most of the experiments, the dipole field in the QMF was applied from one pair of adjacent poles to the opposite pair of adjacent poles. As a result, the application of a sinusoidally varying potential in the dipole configuration produces a potential in the interior of the mass filter that is a complicated function of x and y. However, near the axis of the mass filter, the actual shape of the poles exerts a minor influence on the potential, and the latter can be represented to a fair degree of accuracy as the sum of the two dipole potentials, each across opposite poles separated by $2r_0$ but oriented 90° from one another.

A typical experiment to determine the resolving power of the mass filter involves measuring resonance curves, i.e., the transmitted Cs^+ or UF_6^- ion flux as a function of V_1 for fixed ν_2 and V_2. These curves are functions of input flux and other experimental conditions, such as the magnitudes of ν_1, ν_2, and V_2, the manner of forming and injecting the plasma into the mass filter, the cross-sectional area of the plasma as it enters the mass filter, and the arrangement of elements for extracting and detecting transmitted ions. Experiments were again conducted at two quadrupole frequencies, 0.8 and 0.4 MHz. The results of these experiments will be discussed separately, beginning with those at $\nu_1 = 0.8$ MHz.

In Fig. 14 confinement and resonance curves for Cs^+ at the relatively low peak output current of 0.2 μA are displayed. These results were obtained with the crossed-beam method of plasma injection and with extraction and detection by a Faraday cup formed by four lens elements and a back plate, all at − 100 V. Three prominent features in the resonance curve are observed in Fig. 14. The deep resonance at $V_1 \simeq 6$ kV corresponds to the expected Cs^+ resonance. The dip at ~ 16 kV corresponds to the UF_6^- resonance, but here appears as a loss in transmitted Cs^+ flux. The loss of Cs^+ under conditions where the dipole field is ejecting UF_6^- is a desired effect of space-charge coupling. These results demonstrate that oppositely charged ions do in fact accompany the ejected ions at resonance to preserve space-charge neutrality. The two resonances in the Cs^+ resonance curve

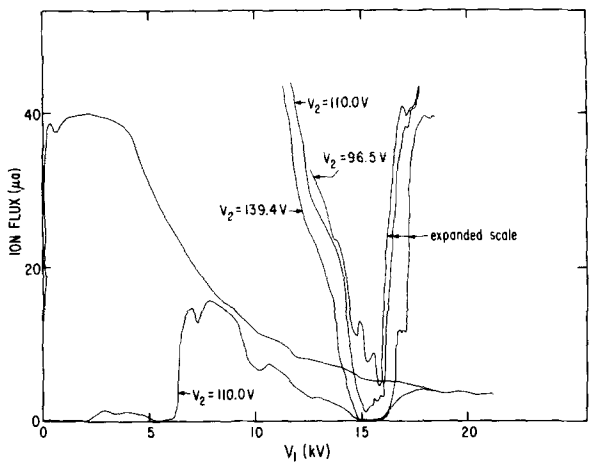

FIG. 16. Measured confinement and resonance curves for UF_6^- at high-ion flux, for three values of the dipole voltage. The crossed-beam mode of plasma injection was used.

are observed at peak output currents down to 0.01 μA, although the depth of the UF_6^- resonance decreases as the throughput decreases. At even lower fluxes, the plasma density is so low that the forces resulting from charge imbalance cannot overcome the quadrupole confining field at the UF_6^- resonance. The third feature in Fig. 14 is the sharp structure at $V_1 = \sim 2$ kV. It was first thought that this feature might suggest the presence of F^- as an impurity species in the plasma. However, measurement of the ion content of the plasma (see Sec. IV A.) detected no F^- at all. The structure at ~ 2 kV is most likely the beginning of a complex ion-loss mechanism at low V_1, which increases dramatically at higher throughput (see below).

In Figs. 15 and 16, confinement and resonance curves for UF_6^- are displayed for peak output fluxes of 4 and 40 μA, respectively. These results were also obtained with the crossed-beam method of plasma injection and the same extraction and collection geometry described above for the Cs^+ curves, except that in the present case the voltage on the extraction and collection elements was changed from -100 to $+200$ V. In addition, the collimator of the UF_6 beam was a factor of 5 larger in diameter than that in the previous experiments, which results in an injected plasma less narrowly focused about the axis of the mass filter. (The effect of collimator size, however, is not thought to be large.) The confinement curves in each of the two figures display the falloff at large V_1 due to the manner of plasma injection, and as discussed in Sec. V, reflects a reduced plasma flux *into* the mass filter itself and not a loss of confinement.

The resonance curves at these higher flux levels are qualitatively more complex than those shown in Fig. 14 and that expected from low-density theory. In addition to the two resonances, Fig. 15 shows a broad loss of UF_6^- transmission at values of V_1 below each resonance, and especially below the Cs^+ resonance. If the throughput is increased about an order of magnitude, then these broad-loss features completely erode the low-V_1 side of each resonance, as seen in Fig. 16. Furthermore, the high-V_1 side of UF_6^- resonance is less sharp, and the magnitude of the dipole voltage V_2 necessary to decrease the minimum of the resonance to zero transmission substantially increases. High values of V_2 also tend to create ledges on the high-V_1 side of the resonance, which severely degrades the resolving power of the mass filter. The Cs^+ resonance curve behaves in a similar fashion at comparable throughputs.

Changing the manner of plasma injection from crossed to merged beam, with H_2 carrier gas, resulted in a dramatic improvement of the confinement curves. Unfortunately, the improvement in the resonance curves was not as great. In Figs. 17 and 18, confinement and resonance curves for both low- and high-input fluxes are shown for merged-beam in-

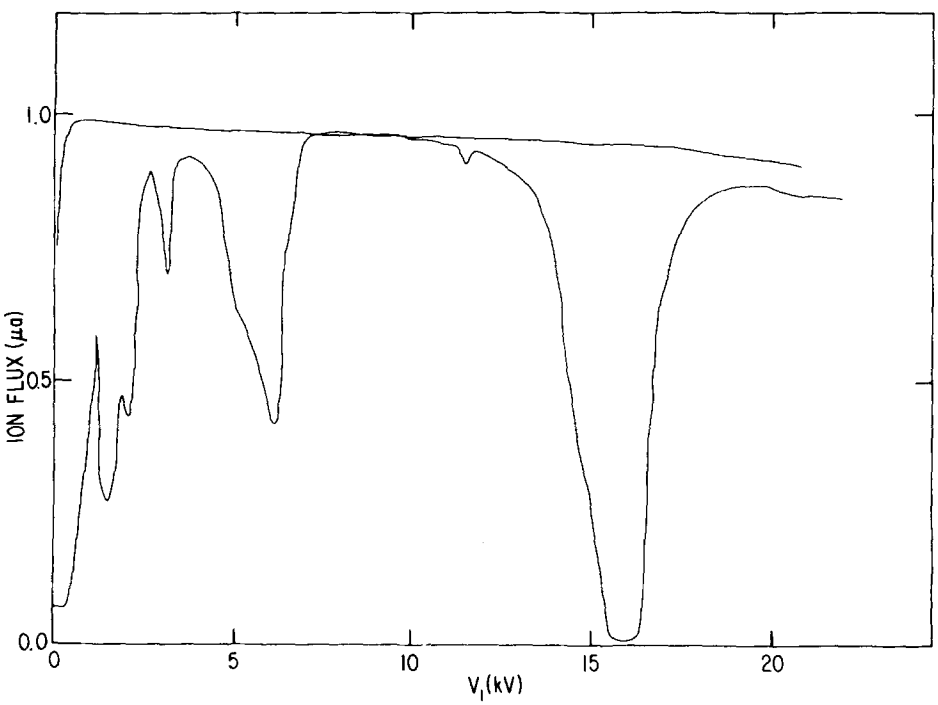

FIG. 17. Confinement and resonance curves for UF_6^- at low-ion flux, with the merged-beam mode of plasma injection.

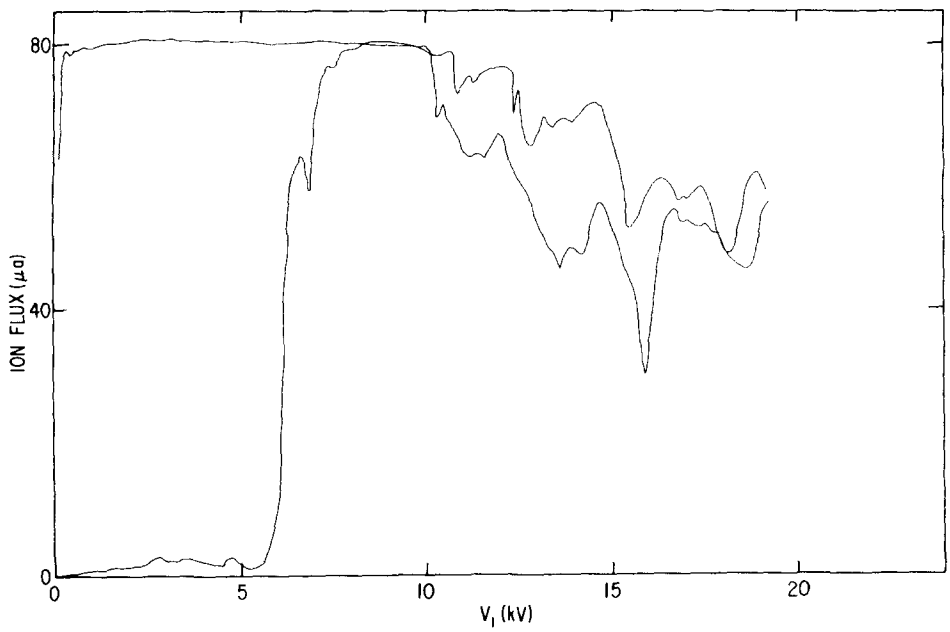

FIG. 18. Confinement and resonance curves for UF_6^- at high-ion flux, with the merged-beam mode of plasma injection.

jection, with H_2 carrier gas. Detection was by a $+200$-V Faraday cup formed by two cylindrical lenses and a back plate. At input fluxes corresponding to a peak output current of 1 μA (Fig. 17), the resonance curve for UF_6^- shows the expected two resonances and a broad loss of transmission below the Cs^+ resonance. The steepness of the high-V_1 side of the UF_6^- resonance is superior to that of the resonance curve in Fig. 15, in part because of the more nearly square bottom of the resonance obtained by increasing the value of V_2. At higher output currents, much higher V_2 voltages are needed to lower this resonance to the base line. Even at a relatively small value of V_2, as is shown in Fig. 18, the broad loss of transmission on the low-V_1 side of each resonance is very much in evidence. The causes of these transmission losses will become apparent from the theoretical modeling described in Paper II, Sec. VI.[2] (See also Sec. VIII of this paper.)

Comparison of the results of the merged- and crossed-beam experiments indicates that, for low- or high-input fluxes, merged-beam injection gives resonances of somewhat better quality than crossed-beam injection, although the trend toward degraded resonances with increasing flux persists. The origin of this difference is probably related to a certain degree of space-charge blowup of the plasma, in the case of crossed-beam injection, in the region between where the ions are formed and where they enter the mass filter. The larger size of the plasma as well as the increasing radial energy induced by the quadrupole fringe field would tend to degrade the quality of the resonance. These effects would tend to increase with increasing plasma density for crossed-beam injection, but are absent for merged-beam injection.

The effect of variation of the extraction and detection geometry on the sharpness of the UF_6^- resonance is seen in Fig. 19. Here, a four-element lens system split evenly between Stages III and IV and a back plate in State IV constituted the extraction/detection system. The elements in Stage IV were held at a common bias of 2 kV to form a Faraday cup for measuring the ion flux. The biases of the first two elements were varied, and the corresponding measured resonance curves in Fig. 19 have been labeled accordingly. As shown in the figure, at high fluxes the large values of V_2 necessary to drive the resonance to zero transmission frequently produce ledges in the high-V_1 side of the resonances. The results in Fig. 19 show that the ledges can be affected by changing the extraction field. A field produced by high voltage on the first lens and even higher bias on the second lens creates the sharpest resonances measured in Stage IV. This is in contrast to confinement curves, where optimum extraction required the first lens to be at low or even negative bias (see Sec. V).

Even with merged-beam injection, H_2 carrier gas, and optimized conditions of extraction, the resonances were

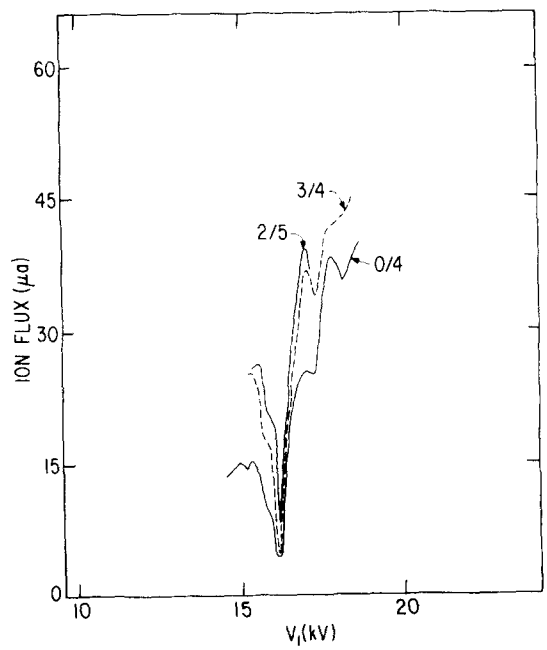

FIG. 19. Resonance curves for UF_6^- at high-ion flux, for three different bias conditions (in kV) on the first two extraction elements.

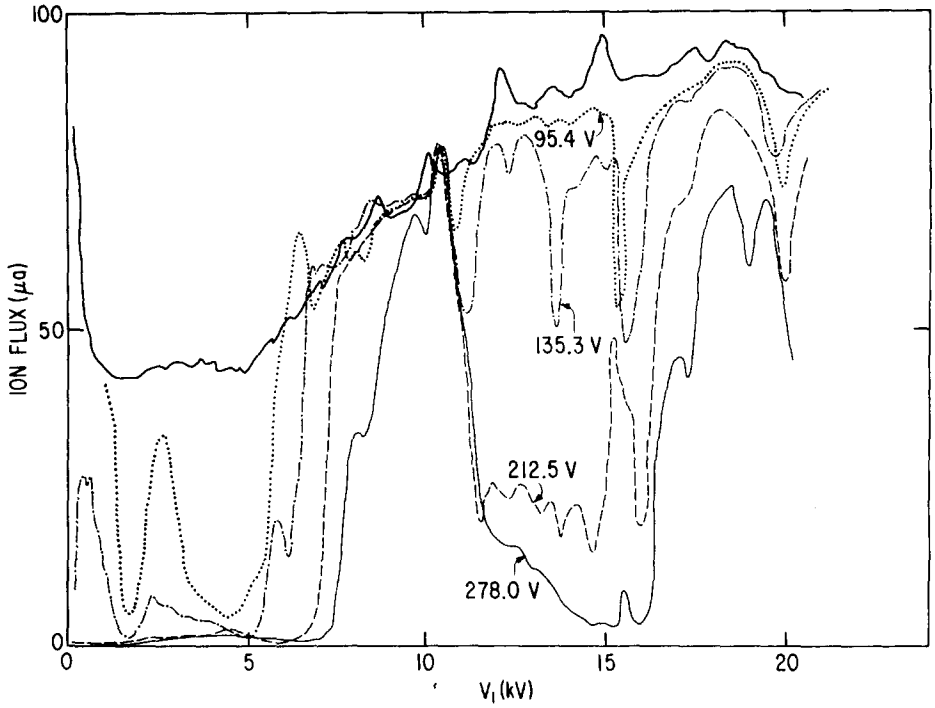

FIG. 20. Confinement and resonance curves for UF_6^- at high-ion flux, for four different dipole field strengths. Merged-beam plasma injection was used.

poor at the high fluxes ($\sim 100\,\mu$A). In Fig. 20 typical resonance curves for a peak output current of 97 μA are displayed. Detection was by a Faraday cup in Stage IV at 2 kV, and extraction was by a two-element lens system in Stage III, with the first lens at 3 kV and the second at 4 kV. The minimum in the confinement curves and subsequent rise at higher V_1 is a result of the competition between the space-charge blowup of the extracted ions (which dominates at low V_1) and the confining force of the exit fringe field (which dominates at high V_1). This was discussed in Sec. V. As the figure shows, at relatively low values of V_2 the UF_6^- resonance is steep but not deep, and the loss of flux at values of V_1 below the Cs^+ and UF_6^- resonances is already quite apparent. As V_2 increases, the high-V_1 side of the Cs^+ resonance shifts to higher values of V_1, while the low-V_1 side is completely eroded by broad loss of transmission. At the same time, the UF_6^- resonance deepens, its minimum shifts to higher values of V_1, the high-V_1 side of the resonance becomes less steep, and the low-V_1 side is eroded by a broad side of transmission. At the high values of V_2 necessary to reduce the resonance to zero transmission, the center of the resonance has moved ~ 1 kV up in V_1, the low-V_1 side of the resonance has been almost completely destroyed, and ledges have appeared on the high-V_1 side of the resonance.

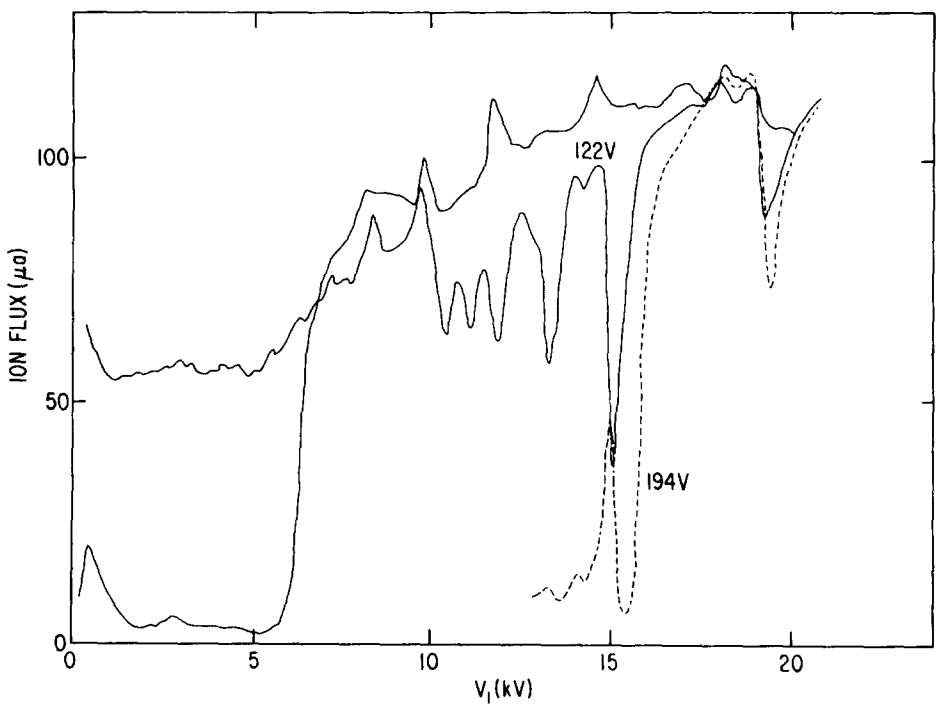

FIG. 21. Confinement and resonance curves for UF_6^- at high-ion flux, for two values of the dipole voltage, with use of a square-wave dipole field.

The UF_6^- resonance could be somewhat improved by applying a dipole field in the form of a square wave rather than a sine wave. In effect, additional frequencies are thereby added to the dipole oscillation so as to change the sine wave rise and fall of voltage into rapid inversion of the sign of a fixed dipole peak voltage. In Fig. 21 the resonance curves for two different values of V_2 are shown for a peak output current of 120 μA. The injection and detection systems were the same as in the previous figure, but the extraction was slightly modified to 3- and 5-kV bias, respectively, on the two lens elements in Stage III. The same basic effects of V_2 are present, i.e., erosion of the low-V_1 side of each resonance by broad loss of transmission, and shift of the center of the resonance to higher values of V_1, although erosion of the UF_6^- resonances appears to be less severe for the case of the dipole field applied as a square wave. The high-V_1 side of the resonances are also steeper than in the previous figure, even though the peak current has been increased by 20%.

Variation of the frequency of the dipole field, whether in the sine wave or square-wave mode, produced surprising effects. In Fig. 22 the region of the UF_6^- resonance is displayed for 80–100-μA peak output current, for six sets of values for ν_2 and V_2. The extraction-detection system [the one employed in sample collection (see Sec. VII)] was composed of two lenses in Stage III at 3 kV, two lenses in Stage IV at 1 kV, deflection of the UF_6^- by the hemicylindrical deflector biased, respectively, at -1 and $+3$ kV, and a 15-cm-diam circular ion detector biased at 5 kV. On varying ν_2 over a range of 0.8 kHz with V_2 fixed or on varying ν_2 over a range of 6.5 kHz with V_2 varying by only $\pm 3.5\%$, the resonance was observed to deepen dramatically near a particular ν_2. Furthermore, the minimum of the resonance did not appear to move appreciably with variation of ν_2, even though the theoretical expectation is that it should shift to higher values of V_1 by amounts directly proportional to the increases in ν_2. The results in Fig. 22 imply the existence of frequency "windows," within which the resonance is very steep. The same effect was observed, although less dramatically, in experiments with the simpler extraction-detection system of the preceding figures.

In addition to variation of V_2, ν_2, and the waveform, the method of applying the dipole field was changed. All the results shown previously in this paper were obtained with the dipole field applied diagonally from one pair of adjacent poles to the opposing pair. The dipole field can also be applied across only *one* pair of poles, such that the field is that of a dipole lying in the plane connecting the two poles. From the results of Paper II, Sec. V,[2] ions may be expected to be ejected along the direction of the dipole. Since ions are actually ejected only when they strike the poles or more distant support structures, ejection by the dipole field pointing in the direction of a pole may be qualitatively different from ejection by the field of a dipole pointing into the space between two poles. However, experiments with the dipole field across a single pair of poles produced essentially the same resonant structures as described above, except that higher values of V_2 were needed to reduce the minimum of the resonance to low transmission.

The effect of initial plasma size on the resonance was also examined by variations in the size of the collimator for the UF_6 beam. The crossed-beam method of plasma injection was used with extraction and detection by a Faraday cup formed by four-lens elements and a back plate at a common voltage. Collimator sizes of 2, 6, and 10 mm diameter for peak currents of 2–8 μA for detection biases of 100–300 V were examined, although not in a systematic fashion. Only minor changes in the depth and steepness of the resonances were observed. This is similar to the results for confinement. Both sets of experiments indicate that because of fringe fields and density-dependent space-charge forces, the plasma size for most of its transit through the QMF is little correlated with its initial size.

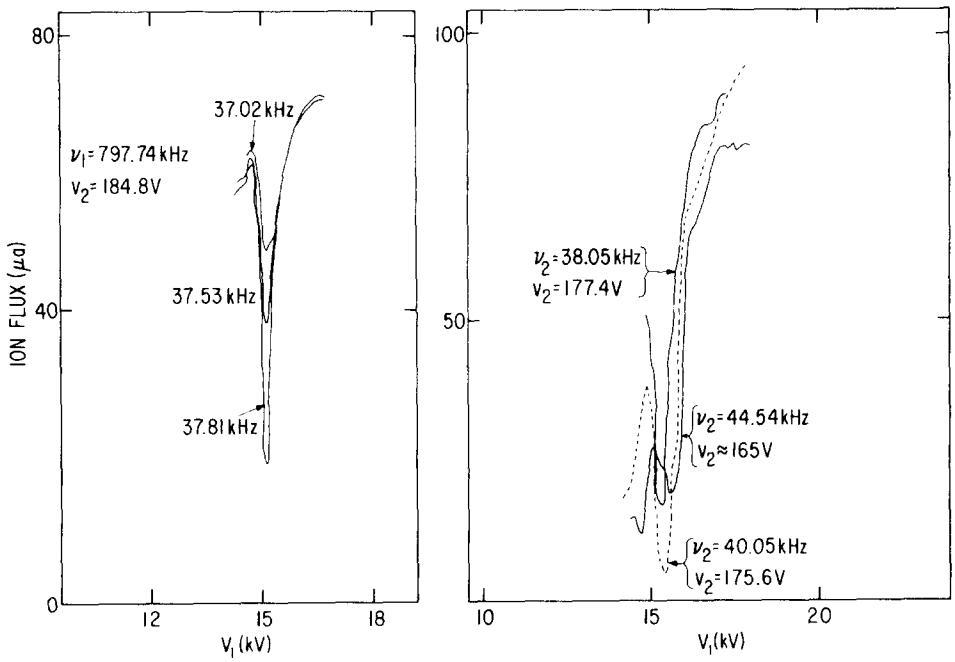

FIG. 22. Resonance curves for UF_6^- as a function of the dipole field frequency, showing the existence of frequency "windows."

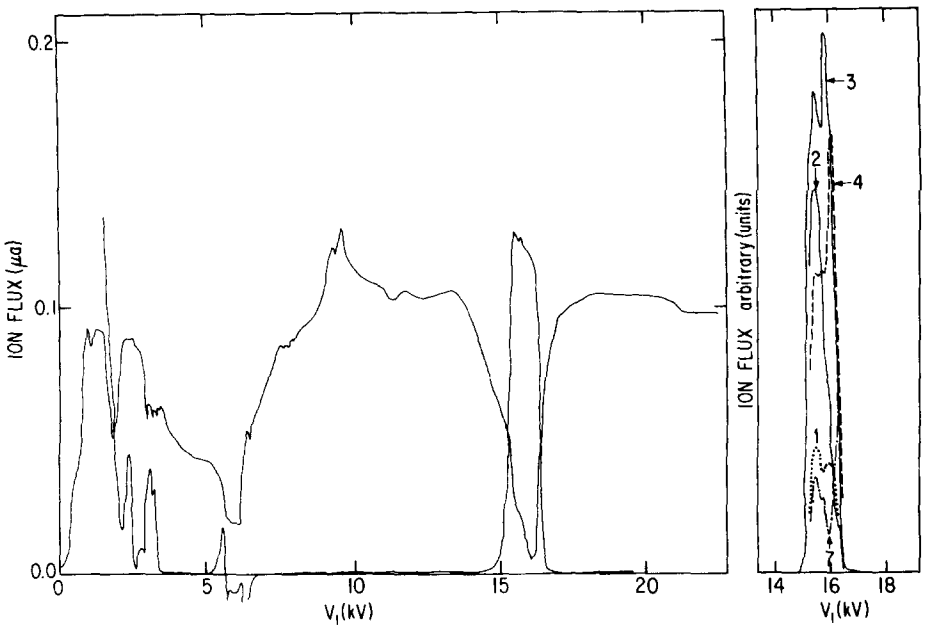

FIG. 23. Resonance curves for UF_6^- at low-ion flux, as determined by the exit Faraday cup and also by all side detector plates (left frame), and by several individual side detector plates (right frame).

The spatial distribution of ejected ions was inferred from several sets of experiments in which ion currents were measured by collection plates placed along the side and around the front of the mass filter. One side detector plate was positioned adjacent to each ten centimeters of quadrupole length. (They were labeled 1–10 starting from the front of the mass filter.) Because of interfering support structures, the plates were not all equally distant from the axis of the QMF, and they had different fringe fields. Ion-collection efficiency by each plate was therefore not constant. Only the crossed-beam injection method was used here, and detection of transmitted ions was by a Faraday cup arrangement. In Fig. 23 (left frame), the resonance curves for UF_6^- as measured by the exit Faraday cup (at $+300$ V) and by all the side plates together, are displayed for a peak output current of ~ 0.1 μA. At both resonances a surge of flux to the side plates occurred. In the vicinity of the Cs^+ resonance, both positive and negative signals were registered on plates biased to $+300$ V. It appears that the Cs^+ ions are ejected with considerable energy. As shown in Fig. 23 (right frame), the distribution of currents on several of the plates at V_1 near the UF_6^- resonance seems to imply that the bulk of the UF_6^- ions are ejected in the first half of the mass filter.

To summarize the results for $\nu_1 = 0.8$ MHz:

(1) Increased plasma density significantly degrades the resolving power of the mass filter, introduces substantial transmission loss over a broad range of values of quadrupole voltage, and requires the use of higher dipole voltages to reduce the minimum of the resonance to very low transmission.

(2) The resolving power is somewhat affected by the extraction-collection geometry and voltages, the choice of a square-wave versus sine wave dipole field, the magnitude of the dipole frequency, and the initial size and off-axis velocity of the plasma, as determined by the diameter of the UF_6 beam collimator, and the method of plasma injection.

(3) The best method for extracting ions of one charge sign into Stage IV with the preservation of the steepest possible resonance is by strongly biased extraction lenses in Stage III. Furthermore, the magnitude of the extraction voltage required for good resolution increased with the flux, and is already several kilovolts at ~ 100 μA.

(4) Square-wave dipole fields produce somewhat steeper resonances than do sine wave fields.

(5) The sensitivity of the quality of the resonance to dipole frequency indicates the presence of frequency windows into the plasma.

(6) The bulk of the ejected ions at resonance are ejected through the sides of the front half of the mass filter.

(7) Significant space-charge effects are absent at output currents of ~ 0.01 μA or less.

The experiments performed with $\nu_1 = \sim 0.4$ MHz all were with the merged-beam injection mode, a 10-mm colli-

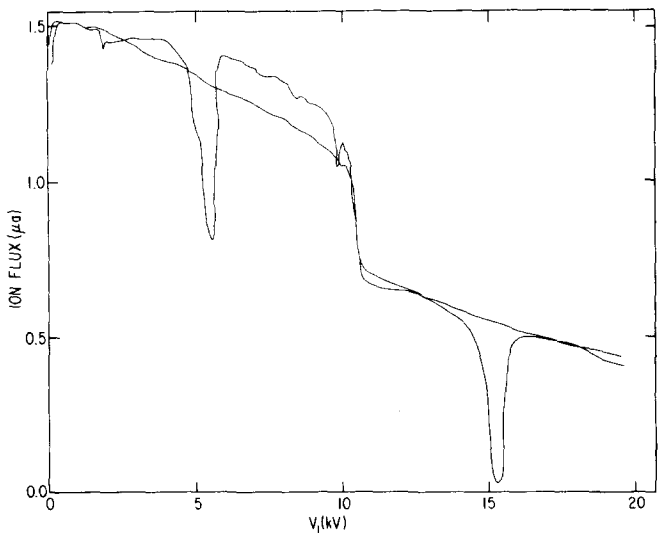

FIG. 24. Confinement and resonance curves for UF_6^- at low-ion flux, with use of the merged-beam mode of plasma injection and a square-wave dipole field. ν_1 was ≈ 0.4 MHz.

mator for the UF_6 beam, and square-wave dipole field. Typical resonance curves for both low- and high-peak output currents are displayed in Figs. 24 and 25, respectively. The extraction system was that used for sample collection (see Sec. VII and Fig. 2), and consisted of two Stage III lens elements biased to 3 and 5 kV, respectively, two Stage IV lenses at 1 kV, the hemicylindrical deflector, and detection by the sample collector at 2 kV. The resonance curve for UF_6^- at low flux in Fig. 24 shows the resonances at the Cs^+ and UF_6^- positions, and the drop-off frequently seen on the confinement curve at 0.4 MHz (see Fig. 13). In contrast to Fig. 15 for $\nu_1 = 0.8$ MHz, at about the same peak output current there is no broad loss of transmission at values of V_1 below the Cs^+ resonance,and the UF_6^- resonance is somewhat sharper. At high flux, the resonance curve for UF_6^- in Fig. 25 shows no broad loss of transmision below the UF_6^- resonance, in contrast to the results for $\nu_1 = 0.8$ MHz (see Fig. 21). The off-resonance portions of the resonance follow the confinement curve. The UF_6^- resonance is well formed, with no displacement of the center or ledge formation with increasing V_2. However, the resonance is also broader, in spite of the fact that it requires somewhat smaller values of V_2 to reduce the minimum of the resonance to very low values of transmission. Thus, decreasing ν_1 to allow confinement of only UF_6^- and increasing ν_2 removes the broad loss of transmission below each resonance, and produces well-formed UF_6^- resonances over all fluxes, but at the price of broader resonances at high flux. Variations in the extraction field do not substantially affect this conclusion. In addition, sensitivity of the resonance to the frequency (i.e., frequency "windows") or to the character (sine wave or square wave) of the dipole field was not observed at $\nu_1 = 0.4$ MHz.

VII. APPLICATION TO URANIUM ISOTOPE SEPARATION

The experimental results in Sec. VI suggest that the resolving power of the QMF deteriorates markedly with increasing plasma flux. This is a direct result of the increasing width of the resonances along with the frequent appearance of shoulders on both the high- and low-voltage sides of the resonances. Despite these characteristics, attempts were made to separate $^{235}UF_6^-$ from $^{238}UF_6^-$ by selectively ejecting the heavier $^{238}UF_6^-$ component, leaving the lighter $^{235}UF_6^-$ confined within the mass filter.

Low-density theory suggests that such a separation would occur if one operates the mass filter at a quadrupole voltage V_1 slightly above that corresponding to the minimum of the $^{238}UF_6^-$ resonance, i.e., at a position where the $^{238}UF_6^-$ transmitted flux is increasing rapidly with increasing V_1. Since the $^{235}UF_6^-$ resonance curve is shifted to lower values of V_1, relative to that for $^{238}UF_6^-$ (assuming low-density theory to be applicable), such an operating point should result in the preferential ejection of $^{238}UF_6^-$ over $^{235}UF_6^-$, and consequently a transmitted product enriched in $^{235}UF_6^-$.

Two different experimental setups were used to measure the isotopic composition of the throughput of the mass filter. For low fluxes of UF_6^-, *in situ* isotopic analysis was performed on the throughput by deflecting the transmitted ions into a commerical analytical quadrupole mass spectrometer. In the high-flux regime, the transmitted ions were deflected onto an efficient liquid-N_2 cold trap. The collected material was later removed from the trap and mass spectrometrically analyzed, a procedure which determined both the

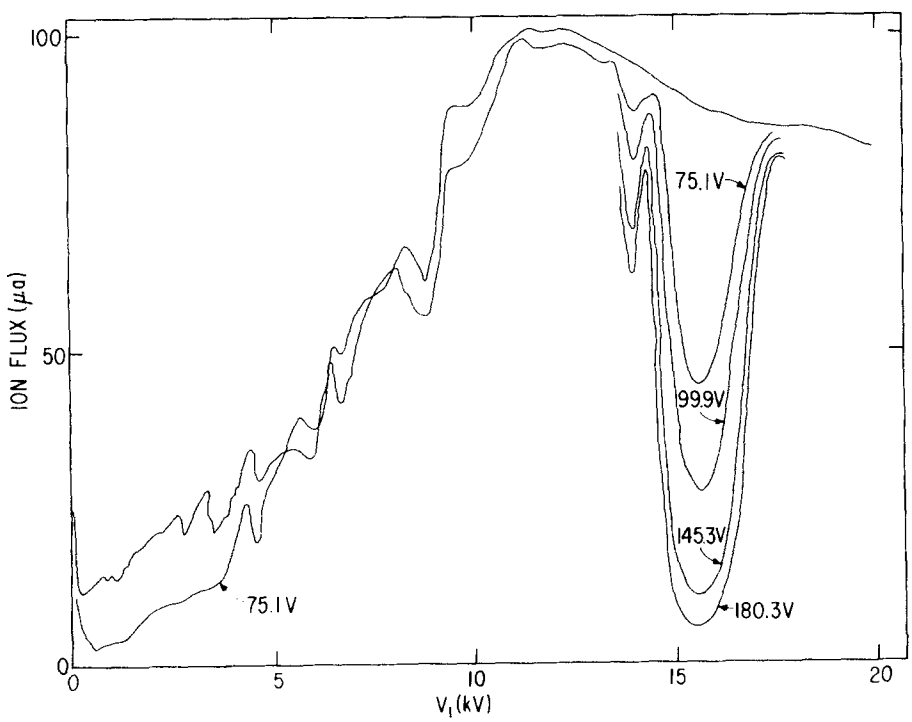

FIG. 25. Confinement and resonance curves for UF_6^- at high-ion flux, the latter for four different dipole voltages. ν_1 was $\simeq 0.4$ MHz.

size of the sample and the $^{235}U/^{238}U$ isotopic ratio.

In the low-flux experiments, the negative ions which passed through the mass filter in Stage III were extracted into Stage IV, deflected through 90° by two high-transmission grids set at 45° to the beam line, and focused onto the entrance of a commerical quadrupole mass spectrometer (Extranuclear Laboratories Model 162-8) equipped with a channeltron for ion counting. In Table I we present the isotopic fraction of $^{235}UF_6^-$ in the transmitted ion flux for each of three settings of the quadrupole voltage, V_1. The ^{235}U enrichment varies from ~5% to 45% as the operating voltage is set at various values relative to that for exact resonance of $^{238}UF_6^-$. (The calculated position of the $^{235}UF_6^-$ resonance was 15.44 kV.) Thus in the low-flux regime the mass filter, as expected, achieves significant mass separation. The highest enrichment, again as expected, was observed when the operating point was just above the voltage corresponding to the minimum throughput of $^{238}UF_6^-$. In this experiment, the ion beam was relatively narrow, as the Stage II collimator was only 2 mm in diameter. Also, the UF_6^- flux (~0.1 μA) was low enough so that space-charge effects were minimal. In addition, the beam geometry and operating parameters of the mass filter were such as to provide for a ratio of ion transit time to beat period higher than that required for complete separation of the two isotopes.

Macroscopic samples of separated product were collected with the experimental arrangement shown in Stage IV of Fig. 2. The throughput of the QMF was focused into Stage IV by the two-element lens system at the exit of the QMF. Once into Stage IV, the UF_6^- ions were slowed and positioned by the split-element lens system, and then deflected ~45° by a deflecting and focusing field formed by voltages on wires drawn taut on two hemicylindrical frames. The deflected ions passed through the wire structure, and were then accelerated into a fin trap, maintained at high-positive potential and cooled to liquid-N_2 temperature. After the collection period, which varied from 0.7 to 4.3 h, Stage IV was isolated and vented with moist N_2, and the fin trap was removed. The uranium was etched from the aluminum fins by dilute HCl, concentrated by evaporation, and mass spectrometrically analyzed for ^{235}U and ^{238}U contents.

In all of these experiments, the initial UF_6^- flux was in the range 200–300 μA. Isotopic separation was again accomplished by adjusting conditions to a preselected operating point on the $^{238}UF_6^-$ resonance curve. This resonance curve was determined from the ion flux to a hemicylindrical detector plate (ion monitor in Fig. 2) which could be moved into an appropriate position between the deflector and the fin trap.

TABLE I. Isotopic analysis of QMF throughput (0.1-μA UF_6^-).

Quadrupole frequency (kHz)	Dipole frequency (kHz)	Quadrupole voltage (kV)	Dipole voltage (V)	$^{235}UF_6^-$ fraction
804.82	37.10	15.57	90.0	0.21
804.82	37.10	15.67	90.0	0.45
804.82	37.10	16.27	90.0	~0.05

TABLE II. Isotopic analysis of QMF throughput (200–300-μA UF_6^-).

Quadrupole frequency (kHz)	Dipole frequency (kHz)	Quadrupole voltage (kV)	Dipole voltage (V)	Measured $^{235}U/^{238}U$ ratio
798.19	38.13	15.40[a]	200	0.006 31 (± 0.000 06)
797.61	38.03	15.37[a]	181	0.006 34
797.72	37.53	15.03[b]	187	0.006 59
797.21	38.01	15.61[c]	193	0.006 54
797.46	38.02	14.51[d]	34	0.006 80
411.43	73.82	16.28[e]	160	0.005 48
411.69	73.56	15.05[d]	35	0.007 01

[a] Indicated voltage is 130 V above the minimum of the $^{238}UF_6^-$ resonance.
[b] Indicated voltage is 170 V below the minimum of the $^{238}UF_6^-$ resonance.
[c] Indicated voltage is 180 V above the minimum of the $^{238}UF_6^-$ resonance.
[d] Indicated voltage is 150 V below the minimum of the $^{238}UF_6^-$ resonance.
[e] Indicated voltage is 870 V above the minimum of the $^{238}UF_6^-$ resonance, which was quite broad; operating point was at ~80% ejection relative to that at the minimum.

The detector was also used to monitor the position of the operating point periodically during the period of sample collection.

The results of the sample-collection experiments are compiled in Table II. The collected samples were typically ~0.5 mg in size. As the data show, the transmitted product was *depleted* in ^{235}U in each case. However, neutral UF_6 collected on the end trap (see Fig. 2) gave a $^{235}U/^{238}U$ ratio in agreement with the natural abundance (i.e., 0.00718). Depletion was observed on the high-voltage side of the resonance where enrichment was expected, on the low-voltage side of the resonance where depletion was expected, as well as at an operating point relatively far up on the resonance shoulder where little separation was expected. Depletion occurred at the high quadrupole frequency (~0.8 MHz), where the Cs^+ ions are within the stability diagram and the plasma is stable in the absence of the dipole field, as well as at the low quadrupole frequency (~0.4 MHz), where the Cs^+ is outside the stability diagram and is lost from the plasma in the absence of the dipole field (see Fig. 12).

The above results show quite clealy that the theory of rf quadrupole operation in the nonplasma (low density) range is not appropriate for the plasma regime. The observation of depletion throughout the resonance region suggests that the complicated interactions of the ion-pair plasma, the quadrupole and dipole fields, and the extraction fields must give rise to a selective ejection of the lighter mass component of the $^{235}UF_6^-/^{238}UF_6^-$ mixture. Calculations on plasma confinement at the higher plasma densities in the absence of a dipole field (see Paper II, Sec. III D.) indicate a greater loss of the Cs^+ vs UF_6^- over the whole range of quadrupole voltages V_1. If this effect is also applicable to the $^{235}UF_6^-/^{238}UF_6^-$ mixture, a preferential loss of $^{235}UF_6^-$ might be observed even in the absence of the dipole field. Collection experiments under these conditions, however, were not performed. With the addition of a dipole field, the calculations in Paper II give preferential ejection of Cs^+ or UF_6^- depending on the value of V_1. In the region of the UF_6^- resonance, however, ejection of Cs^+ was again favored, despite the fact that the

UF_6^- was nominally being ejected. This again suggests a greater loss of the lighter mass component. Although the physical origin of this effect is not clear, the experimental observation of depletion of $^{235}UF_6^-$ from the transmitted ions is in qualitative agreement with the implications of the theoretical results.

VIII. DISCUSSION

In the following discussion, we will consider the two fundamental issues which prompted the experimental studies. First, what are the throughput limitations associated with passing an ion-pair plasma through a QMF, and second, how does the presence of a plasma affect the mass-resolving power of the mass filter? In the discussion, we will include results obtained from the theoretical studies given in Paper II,[2] to which the reader is referred for a more complete discussion. We consider confinement of the plasma in the rf quadrupole field first.

The behavior of a plasma in a time-varying external electric field depends on the relationship between the frequency of the applied field ν_1, the effective collision frequency of ions within the plasma ν_c, and the plasma frequency ν_p. The latter is given by [14] $\nu_p = (\frac{1}{2}\pi)(4\pi e^2\rho/\mu)^{1/2} = 21.4p^{1/2}$ $\sec^{-1}$ for a Cs^+-UF_6^- plasma, where μ is the Cs^+-UF_6^- reduced mass and ρ is the positive or negative ion density in cm^{-3}. It is easy to show that at the maximum ion densities obtained in our experiments $\nu_c \ll \nu_1$. Under these conditions, for densities such that $\nu_p \ll \nu_1$, the plasma behaves as a nearly transparent dielectric.[15] For densities such that $\nu_p \gg \nu_1$, the plasma is opaque and highly reflective.

From a physical point of view, for $\nu_p \gg \nu_1$ the plasma oscillates in phase with the applied field, producing an oscillating space-charge force equal in magnitude but opposite in direction to the applied field, resulting in a zero net field within the plasma (in the absence of thermal motion of the ions and of density variations of the ion distribution). Here one usually speaks of a lack of penetration of the applied field into the plasma. What is important here is that the space-charge forces are comparable in magnitude to the applied forces. For $\nu_p \ll \nu_1$ on the other hand, the plasma is too sluggish to follow the variations in the applied field, and the amplitude of the space-charge forces decreases with decreasing density resulting in a nonzero field within the plasma.

In Sec. IV we estimated that the highest ion densities produced in the experiments were $\sim 1.1\times 10^{10}$ ions/cm^3, which is the calculated ion density in the region where the ions are formed in the crossed-beam mode of plasma injection. From this density,we obtain $\nu_p = 2.24$ MHz, which is approximately three times the highest rf quadrupole frequency studied experimentally (~ 0.8 MHz).

However, considerable blowup of the plasma before it enters the mass filter itself is likely, due to both thermal blowup as well as to complex interactions of the plasma with the entrance fringe field (see below). The thermal blowup is particularly difficult to estimate, since it requires knowledge of the final states resulting from the Cs-UF_6 charge-exchange reaction. While it is thought that UF_6^- is formed in an excited electronic state,[9] the energetics of this reaction are not known, and consequently the internal temperature of the plasma is indeterminant. It is our best estimate that at the highest currents exiting the QMF ($\sim 330\,\mu$A), the plasma frequency is somewhat higher than the applied quadrupole frequency of 0.8 MHz.

The experimental results in and of themselves do not demonstrate a throughput limitation at throughputs up to several hundred microamps. The identification of a throughput limitation is made difficult by the complex effects of entrance and exit fringe fields, which severely distort the confinement curves at high V_1. The distortion is particularly clear in Fig. 8, where effects of the entrance fringe field were eliminated by using merged-beam injection. In this case, a relatively flat confinement curve could only be obtained with a high extraction field, which eliminates the reflection of ions resulting from the exit fringe field. Clearly at the 60-μA flux level, there would appear to be no V_1-dependent loss of confinement within the mass filter itself. Theoretical calculations at this level of throughput (Paper II, Sec. III) also indicate complete confinement, although space-charge forces are already sufficient to significantly distort the ion trajectories.

At the highest throughput shown in Fig.7, it is not clear whether the distortion of the confinement curve is entirely related to fringe-field effects, or in fact, reflects a partial loss of confinement within the mass filter itself. Theoretical calculations performed at the higher throughput levels demonstrate that loss of confinement within the mass filter begins to become significant at throughput levels of $\sim 100\,\mu$A. It is significant to note that this throughput limitation corresponds to an ion density for which the plasma frequency is approximately equal to the applied frequency,and this suggests that the only limitation on plasma confinement is the requirement that the plasma frequency be less than or at most equal to the applied frequency. (Owing to uncertainties in the accuracy of the theoretical calculations and the measurement of ion densities within the mass filter, an upper limit to the throughput based on $\nu_p = \nu_1$ is probably good only to about a factor of 2.)

If a plasma flux in excess of the limiting throughput enters the mass filter (e.g., by the merged-beam injection method), the excess plasma flux must be lost through the sides of the mass filter before the confining action of the applied field can be operative. The theoretical calculations of Paper II[2] elucidate the mechanism for plasma loss. They indicate that while the applied field fails to penetrate into the plasma in the case $\nu_p \gg \nu_1$, a complex interaction of the applied field and the induced space-charge forces shred the plasma at its edges, stripping off layer upon layer of ions until an ion density is reached whereby confinement of the remaining plasma can occur. At densities near $\nu_p = \nu_1$, a more general blowup of the plasma occurs along with shredding of the plasma at its periphery. The blowup and shredding of the plasma occur on a time scale which is small compared to the expected blowup due to thermal or geometrical factors.

The blowup of the plasma when the ion density increases is well documented in the experimental record. It appears as an increasing degradation of the confinement

curves with increasing density caused by the entrance and exit fringe fields. These fields produce axial forces which increase with distance from the axis of the mass filter. At the entrance of the mass filter, radial plasma blowup in the crossed-beam mode of plasma injection exposes the edges of the plasma to the larger axial forces of the fringe field, resulting in much greater reflection of ions at given V_1. Since the axial forces also increase linearly with V_1, reflective loss increases both with density at constant V_1 and with V_1 at constant density (see Figs. 5 and 10). At the exit of the mass filter, reflection of ions due to the exit fringe field is again seen to increase with increasing density (see Figs. 6 and 7). This produces strong oscillation of the throughput with V_1, which to some extent can be removed by a stronger draw-out voltage. These effects again probably reflect an increasing plasma blowup as the $\nu_p = \nu_1$ limit is approached.

In summary, the applied rf quadrupole field acts to rapidly destroy a plasma whose density is such that $\nu_p \gtrsim \nu_1$. The destruction continues until the density is reduced to where $\nu_p < \nu_1$, allowing the applied field to fully penetrate and confine the remaining plasma.

We now turn to consideration of the resolving power of the mass filter in the presence of an ion-pair plasma. It should be noted at the outset that because of the lower frequency of the dipole field ν_2 compared to $\nu_1(\nu_2/\nu_1 \simeq 0.048$ for $\nu_1 = 0.8$ MHz and ~ 0.18 for $\nu_1 = 0.4$ MHz), the density at which $\nu_p = \nu_2$ is much lower than that for the quadrupole field alone (a factor of 430 lower for $\nu_1 = 0.8$ MHz and 31 lower for $\nu_1 = 0.4$ MHz). As a result, the disruptive effect of the dipole field on the plasma, i.e., plasma blowup and the associated shredding at the periphery for $\nu_p \geqslant \nu_2$, would be expected to begin at densities where the quadrupole field itself is acting to confine the ions. [Theoretical calculations (Paper II, Sec. VI)[2] done with only the dipole field applied show the same plasma disruption for $\nu_p > \nu_2$ as observed for $\nu_p > \nu_1$ with only the quadrupole field applied.] As a result, over much of the throughput level studied experimentally, the two fields in a sense act in opposition to each other.

In Sec. VI, it was demonstrated that some degradation of the plasma in a dipole field was observed at as low a throughput as ~ 0.2 μA (for $\nu_1 = 0.8$ MHz), or approximately a factor of 1000 below the maximum throughput observed (see, for example, the dip in throughput at ~ 2 kV in Fig. 14). The destructive effects of the dipole field are first observed at low V_1, due to the nature of the resonance curve. Since the latter was obtained by varying V_1 from 0 to ~ 20 kV, the confining action of the quadrupole field varies from 0 to some maximum effect, while the destructive action of the dipole field (if $\nu_p > \nu_2$) is relatively constant (since V_2 is constant). While this analysis is qualtiatively correct, since the major nonresonance throughput losses occur at low V_1, the experimental results show various "resonance"-type features that occur as the throughput is increased, implying a more complicated interaction of the two fields than that indicated above.

As the throughput increases from 0.2 to 4 μA, and finally to 40 μA (see Figs. 14, 15, and 16), the destruction of the plasma at low V_1 increases from the single dip at 2 kV in Fig. 14 to an almost complete loss of confinement from $V_1 = 0$ to approximately the position of the Cs^+ resonance. In addition, a secondary loss feature appears just below the UF_6^- resonance (see Fig. 15), which at high throughput completely erodes the low-voltage side of that resonance (see Fig. 20 for the sine wave dipole field and Fig. 21 for the square-wave dipole field). Theoretical calculations confirm the existence of these throughput losses, but generally do not reproduce the sharp "resonance"-type features seen, for example, in Fig. 21 just below the UF_6^- resonance. The somewhat severe approximations necessary to make the space-charge calculations feasible probably result in a smoothing out of the finer details of the resonance behavior.

Besides the destructive loss of plasma at low V_1, the Cs^+ resonance curve shown in Fig. 14 also shows a loss in Cs^+ confinement at the UF_6^- resonance. This presumably reflects space-charge blowup of the Cs^+ beam upon ejection of the UF_6^- at its resonance. It occurs, however, at remarkably low throughput considering that 80 μA of UF_6^- could be confined in the absence of the Cs^+ counter ion (see Fig. 13). Clearly, the ejection of the UF_6^- at the UF_6^- resonance and/or the presence of the dipole field significantly affects the confinement of Cs^+ in a way not simply accounted for on the basis of simple estimates of space-charge forces. Indeed, the experimental results generally show space-charge effects at lower ion densities than are predicted by the theoretical calculations (see Paper II, Secs. III and VI).[2]

Given that $\nu_p > \nu_2$ for most of the throughput range studied experimentally, one might well ask why resonance ejection of Cs^+ or UF_6^- occurs at all, since penetration of the dipole field into the plasma under these circumstances is likely to be poor. Experimentally, as the plasma density increased, a considerably larger dipole field strength was required to drive the resonance to zero transmission, demonstrating its decreased effectiveness at the higher densities. Two factors may bear on the above question. First, plasma shielding in the case of $\nu_1 > \nu_p > \nu_2$ may well be disrupted by the simultaneous presence of the rf quadrupole and dipole fields, leading to partial penetration of the dipole field into the plasma. Second, resonant absorption from the dipole field may occur primarily for ions located near the periphery of the plasma, resulting in a kind of shredding of the plasma near its edges, a process which would be greatly enhanced at the Cs^+ or UF_6^- resonance. Measurements at low throughput of the loss of UF_6^- through the sides of the mass filter showed not an abrupt loss at a particular axial position, but a broad loss of transmission over the entire length of the mass filter, peaking in the upstream half, perhaps suggesting a shredding-type mechanism.

The influence of space-charge forces on the widths of the resonances is somewhat difficult to decipher from the experimental results. Only in the case of 0.4 MHz is there a clear indication of resonance broadening with increasing ion density (compare Figs. 24 and 25). Such broadening is not unexpected. Any effect which would alter the fundamental mode of ion motion (to which ν_2 is set) would be expected to induce broadening in the resonances. Clearly, space-charge forces which are comparable with the applied forces would be expected to significantly alter the fundamental frequency

of ion motion, or perhaps more correctly, induce a much larger spectrum of frequencies necessary to describe the behavior of the ions. As ion ejection increases as a resonance is approached, the space-charge forces diminish and the "resonance" frequency moves toward the low-density limit. Thus ejection inevitably occurs over a range of densities, a process which almost certainly contributes to the broadening process.

In the case of 0.8 MHz, both the Cs^+ and UF_6^- resonances certainly degrade with increasing density. But in addition to resonance broadening, secondary loss features appear near the resonances, as well as ledges caused by ion extraction effects, making it all but impossible to separate out the various effects. In addition, sensitivity to the shape of the dipole field (sine wave vs square wave) was significant (compare Figs. 20 and 21), as well as the observation of frequency windows (see Fig. 22). All these features, except for broadening of the resonances themselves, apparently result from the presence of the counter ion, since they were largely absent in the UF_6^- resonance at 0.4 MHz, for which the Cs^+ counter ion was absent.

The degradation of the resonance shape with increasing density clearly demonstrates a severe decrease in mass-resolving power with increasing density. The results of Sec. VII show, in addition, that the presence of sharp features on the resonance curve do not insure a high degree of mass-resolving power. A study which allows continuous detection of different mass components (e.g., $^{235}UF_6^-$ and $^{238}UF_6^-$) is needed to determine accurately the mass dependence of ejected material. Owing to the size of the mass filter used in the present studies and the extremely strong extraction conditions needed at high plasma throughput, such measurements proved, in the present case, to be impractical.

ACKNOWLEDGMENTS

We wish to express our appreciation to L. G. Pobo for his assistance in performing the experiments and to J. Aron, J. M. Nixon, and J. E. Sterling for their aid in designing the apparatus. We thank M. H. Studier for the analysis of the composition of the UF_6 sample. We also thank A. F. Wagner for many informative discussions both during the course of the experimental work as well as in the writing of this paper.

This work was supported principally by the Advanced Nuclear Systems and Projects Division, Advanced Isotope Separations Branch, and also by the Office of Basic Energy Sciences, Division of Chemical Sciences, U.S. Department of Energy, under Contract W-31-109-Eng-38.

[1] See, for example, L. O. Love in *Proceedings of the International Conference on Electromagnetic Isotope Separators and the Techniques of Their Applications*, H. Wagner and W. Walcher, eds. (Zentralstelle für Atomkernenergie–Dokumentation, Leopoldshafen, West Germany, 1970), p. 176.
[2] A. F. Wagner, J. Appl. Phys. **54**, 1755(1983).
[3] P. Davidovits and J. L. Hirshfield, Appl. Phys. Lett. **15**, 290 (1969).
[4] H. J. Doucet and C. Rouille, Vacuum **24**, 527 (1974).
[5] S. Avrillier and J. P. Schermann, J. Phys. (Paris) **38**, 913 (1977).
[6] H. J. Doucet, Phys. Lett. A **33**, 283 (1970).
[7] J. Taillet, *Proceedings of the 7th International Conference on the Phenomena in Ionized Gases*, **1**, 468 (1966).
[8] J. P. Schermann and F. G. Major, Appl. Phys. **16**, 225 (1978).
[9] B. K. Annis and S. Datz, J. Chem. Phys. **69**, 2553 (1978).
[10] N. Abuaf, J. B. Anderson, R. P. Andres, J. B. Fenn, and D. G. H. Marsden, Science **155**, 997 (1967).
[11] W. Paul, H. P. Reinhard, and U. von Zahn, Z. Phys. **152**, 143 (1958).
[12] R. Kohler, W. Paul, K. Schmitt, and U. von Zahn, *Nucleidic Masses* (University of Toronto, Toronto, 1960), p. 507.
[13] M. Mosharrafa and H. J. Oskam, Physica **32**, 1759 (1966).
[14] M. A. Heald and C. B. Wharton, *Plasma Diagnostics with Microwaves* (Wiley, New York, 1965), p. 3.
[15] M. A. Heald and C. B. Wharton, *Plasma Diagnostics with Microwaves* (Wiley, New York, 1965), p. 9.